Acta Universitatis
Lappeenrantaensis
804

Jonna Tiainen

LOSSES IN LOW-REYNOLDS-NUMBER CENTRIFUGAL COMPRESSORS

LUT
Lappeenranta
University of Technology

Jonna Tiainen

LOSSES IN LOW-REYNOLDS-NUMBER CENTRIFUGAL COMPRESSORS

Thesis for the degree of Doctor of Science (Technology) to be presented with due permission for public examination and criticism in the Auditorium 2303 at Lappeenranta University of Technology, Lappeenranta, Finland on the 5th of September, 2018, at noon.

Acta Universitatis
Lappeenrantaensis 804

Supervisors Professor Jari Backman
LUT School of Energy Systems
Lappeenranta University of Technology
Finland

Associate Professor Ahti Jaatinen-Värri
LUT School of Energy Systems
Lappeenranta University of Technology
Finland

Reviewers Professor Ricardo Martinez-Botas
Department of Mechanical Engineering
Imperial College London
United Kingdom

Professor Stephen Spence
School of Mechanical and Aerospace Engineering
Queen's University Belfast
United Kingdom

Opponents Professor Ricardo Martinez-Botas
Department of Mechanical Engineering
Imperial College London
United Kingdom

Doctor of Science (Technology) Arttu Reunanen
R&D Manager, Aeration
Sulzer Pumps Finland Oy
Finland

ISBN 978-952-335-249-0
ISBN 978-952-335-250-6 (PDF)
ISSN-L 1456-4491
ISSN 1456-4491
Lappeenrannan teknillinen yliopisto
LUT Yliopistopaino 2018

Abstract

Jonna Tiainen
Losses in low-Reynolds-number centrifugal compressors
Lappeenranta 2018
64 pages
Acta Universitatis Lappeenrantaensis 804
Diss. Lappeenranta University of Technology
ISBN 978-952-335-249-0, ISBN 978-952-335-250-6 (PDF)
ISSN-L 1456-4491, ISSN 1456-4491

Micro-scale centrifugal compressors and compressors operating at a high altitude suffer from performance deterioration due to low Reynolds numbers. An improvement in the efficiency of a low-Reynolds-number centrifugal compressor could result in increased technological feasibility of micro-scale gas turbines.

The deteriorated performance of a centrifugal compressor due to low Reynolds numbers is usually accounted for in the design process with empirical correction equations published in the literature, but the correction equations do not offer any consideration of whether the efficiency drop can be countered somehow. In this work, the loss generation in low-Reynolds-number centrifugal compressors is investigated theoretically and numerically, and the results are compared to empirical correction equations. A new method, called the hybrid method, is developed to study the boundary layers in the blade passages in closer detail.

The results of this work indicate that the greatest increase in the Reynolds-number losses occurs in the boundary layers near the impeller hub and diffuser surfaces. In addition to the increased boundary layer losses, the results indicate that the tip leakage flow is strengthened with the decreasing Reynolds number, even if the relative tip clearance is kept constant. In order to improve the performance of low-Reynolds-number centrifugal compressors, the boundary layer thickness should be reduced and the tip leakage flow controlled. Passive flow control methods would be better than active ones in the micro-scale compressors due to the less complex structure, but their performance depends on the operating conditions.

Keywords: boundary layer, centrifugal compressor, efficiency, hybrid method, impeller, losses

Acknowledgements

This study was carried out in the Laboratory of Fluid Dynamics at Lappeenranta University of Technology, Finland, between 2014 and 2018, within the "Low Reynolds number kinetic compression" project. The financial contribution of the Academy of Finland is gratefully acknowledged.

I would like to express my sincere gratitude to Professor Jari Backman for offering the possibility for this research, and to Associate Professor Ahti Jaatinen-Värri for encouragement, guidance and support. I would like to offer my special thanks to Associate Professor Aki Grönman for constructive suggestions in the role of "third supervisor".

I would like to express my very great appreciation to Professor Seume and Research group at Leibniz Universität Hannover, Germany, where I got a chance to spend three amazing months in 2015. I am grateful for their hospitality and friendships.

I would like to express my thanks to the reviewers Professor Martinez-Botas and Professor Spence for their valuable comments which helped me to improve my thesis.

My special thanks are extended to Doctor Michael Casey for the suggestion to study the influence of transitional turbulence modelling.

I would like to thank Mrs Sinikka Talonpoika for proofreading.

Finally, I am grateful to my family: dad, Minna, and Veli-Sakari for love and support. This thesis is dedicated to the memory of my mom. I would like to thank Martti and Eija for the close support and drifting my mind away from work. And Samu: thanks for making me smile.

Jonna Tiainen
June 2018
Lappeenranta, Finland

Contents

List of publications

This thesis is based on the following publications, which are referred to as **Publications I-V** in the text. The rights have been granted by the publishers to include the publications in the thesis.

I Tiainen, J., Jaatinen-Värri, A., Grönman, A., and Backman, J. (2016). Numerical study of the Reynolds number effect on the centrifugal compressor performance and losses. *In: Proceedings of ASME Turbo Expo 2016: Turbine Technical Conference and Exposition*. Paper No. GT2016-56036. June 13-17, 2016, Seoul, South Korea.

II Tiainen, J., Jaatinen-Värri, A., Grönman, A., and Backman, J. (2017) Influence of Reynolds number variation method on centrifugal compressor loss generation. *In: Proceedings of 12th European Conference on Turbomachinery Fluid dynamics & Thermodynamics*. Paper No. ETC2017-041. April 3-7, Stockholm, Sweden.

III Tiainen, J., Jaatinen-Värri, A., Grönman, A., Turunen-Saaresti, T., and Backman, J. (2018) Effect of freestream velocity definition on boundary layer thickness and losses in centrifugal compressors. *Journal of Turbomachinery*. 140(5):051003.

IV Tiainen, J., Grönman, A., Jaatinen-Värri, A., and Backman, J. (2018) Flow control methods and their applicability in low-Reynolds-number centrifugal compressors—A review. *International Journal of Turbomachinery, Propulsion and Power*. 3(1):2.

V Tiainen, J., Jaatinen-Värri, A., Grönman, A., Fischer, T., and Backman, J. (2018) Loss development analysis of a micro-scale centrifugal compressor. *Energy Conversion and Management*. 166, pp. 297–307.

The author was the corresponding author and principal researcher in all **Publications**, which were planned together with the co-authors. In **Publications I-III** and **V**, the mesh generation, numerical simulations, post-processing, and analysis of the numerical results were done by the author. The co-authors contributed to the writing of the text and offered guidance and suggestions.

In Publication IV, the author reviewed the literature and was mainly responsible for writing the paper. Dr Aki Grönman and Dr Ahti Jaatinen-Värri participated in analysing the data and contributed also to the writing. Prof. Jari Backman contributed to the funding of the study.

Nomenclature

Latin alphabet

A	area	m^2
a	fraction of Reynolds-independent losses in Eqn. (2.5)	–
a	speed of sound	m/s
b	blade height	m
b	fraction of Reynolds-dependent losses in Eqn. (2.7)	–
B_{ref}	coefficient in Eqns. (2.8) and (2.9)	–
c	absolute velocity	m/s
c	chord length	m
c	coefficient in Eqn. (2.6)	–
C_{d}	discharge coefficient in Eqn. (5.4)	–
C_{d}	dissipation coefficient in Eqn. (2.15)	–
c_{f}	friction coefficient	–
C_{pr}	pressure recovery coefficient	–
c_{p}	specific heat capacity at constant pressure	J/kgK
c_{s}	blade surface length	m
D	diameter	m
f	friction factor	–
GCI_{fine}	fine-grid convergence index	–
h	specific enthalpy	J/kg
K_{p}	total pressure loss coefficient	–
Ma_{U}	tip speed Mach number	–
n	Reynolds-number-ratio exponent in Eqns. (2.5) and (2.7)	–
n	rotational speed	rpm
N_{s}	specific speed	–
p	apparent order of convergence	–
p	blade pitch	m
p	pressure	Pa
q_{m}	mass flow rate	kg/s
q_{v}	volume flow rate	m^3/s
R	specific gas constant	J/kgK
r	radius	m
Re_{c}	chord Reynolds number	–
SF	scaling factor	–
t	tip clearance	m
t^*_{te}	dimensionless trailing-edge thickness	–
t_{te}	trailing-edge thickness	m
U	tip speed	m/s
U_δ	velocity at the boundary layer edge	m/s
U_∞	free-stream velocity	m/s
w	relative velocity	m/s

Z	number of blades	–

Greek alphabet

α	absolute flow angle	$^\circ$
β	relative flow angle	$^\circ$
δ	boundary layer thickness	m
δ^*	dimensionless displacement thickness	–
η	efficiency	–
μ_0	work input coefficient in Eqn. (2.6)	–
ν	kinematic viscosity	m^2/s
ω	angular velocity	rad/s
ϕ	flow coefficient	–
ψ	pressure coefficient	–
Ψ^*	dimensionless energy thickness	–
ρ	density	kg/m^3
ζ	loss coefficient	–

Subscripts

1	impeller inlet
2	impeller outlet
3	diffuser outlet
ave	average
bl	boundary layer
crit	critical
h	hub
ref	reference
r	radial
s	isentropic
s	shroud
s	static
te	trailing edge
tl	tip leakage
t	total
u	tangential

Abbreviations

DES	design point
FB	full blade
LE	leading edge
NC	near choke
NS	near stall

PE	peak efficiency point
PS	pressure side
SB	splitter blade
SS	suction side
TE	trailing edge

1 Introduction

1.1 Background

One of the main objectives of today's research is to develop sustainable ways to utilise the world's energy resources. Affordable and clean energy is set as one of the 17 sustainable development goals by the United Nations (2015). The energy strategies of the European Union aim at improving the energy efficiency and increasing the share of renewable energy sources to 27% by 2030 (the European Commission, 2012a) and cutting greenhouse gas emissions by $80 - 95\%$ from the level of 1990 by 2050 (the European Commission, 2012b). In the energy strategies for 2030 (Huttunen, 2014) and 2050 (the Parliamentary Committee on Energy and Issues, 2014), Finland has committed to the EU targets and aims at increasing self-sufficiency in energy to 55% and the share of renewable energy sources to approximately 50% by 2030, as the share was around 39% already in 2016 (Official Statistics of Finland (OSF), 2017).

The targets set for reducing emissions and ensuring self-sufficiency in energy can be achieved in a cost-effective way by improving energy efficiency (the International Energy Agency, 2017). Globally, the industrial sector accounts for on average 50% of the overall electricity consumption (Vittorini and Cipollone, 2016). In Finland, the share of the electricity consumption of industry was 47% (40 TWh) in 2016 (Official Statistics of Finland (OSF), 2017). Of the overall electricity consumption of the industry, compressors alone account for 15% (Vittorini and Cipollone, 2016). Therefore, the improvement of compressor performance plays an important role in reducing the end-use electricity demand and improving the energy efficiency.

Especially small-scale centrifugal compressors have great potential for efficiency improvement due to their clearly low performance. The small size of a centrifugal compressor (impeller outlet diameter less than 30 mm (Casey et al., 2013)) results in a low Reynolds number, leading to a clearly lower performance than that of a larger counterpart (Casey and Robinson, 2011). For example, a reduction of 96% in the Reynolds number resulted in a 15 percentage points lower efficiency in a centrifugal compressor (Casey, 1985). Centrifugal compressors have been studied in the Laboratory of Fluid Dynamics at Lappeenranta University of Technology since 1981, and the work presented in this thesis continues this tradition by providing information about centrifugal compressors operating at low Reynolds numbers. This work is part of the "Low-Reynolds number kinetic compression" project funded by the Academy of Finland under grant number 274897.

An improvement in the efficiency of a centrifugal compressor operating at a low Reynolds number could result in e.g. increased technological feasibility of micro-scale gas turbines (Martinez et al., 2017). Micro-scale gas turbines (less than $100 - 1000$ kW (Backman and Kaikko, 2011)) could be a potential solution for combined heat and power applications to increase the use of biomass, to reduce greenhouse gas emissions, and to increase self-sufficiency in energy (Martinez et al., 2017; Visser et al., 2012) due to their flexibility

and scalability (Durante et al., 2017). In addition to distributed energy generation, micro-scale gas turbines have also potential in applications requiring a compact, portable power source due to high power density (Dessornes et al., 2014; Epstein et al., 2000); e.g. in mobile devices (Seo et al., 2017), robots (Isomura et al., 2006), and unmanned aerial vehicles (Marcellan et al., 2016). A micro-scale centrifugal compressor could also replace a displacement compressor in small refrigeration systems in order to achieve lower power consumption and weight (Röyttä et al., 2009a).

1.2 Objectives of the study

The objectives of this study are:

1. To study loss generation in low-Reynolds-number centrifugal compressors theoretically and numerically.
2. To develop a method to overcome the challenge of estimating boundary layer thickness in centrifugal compressors.
3. To find out the most significant loss generation mechanisms inside the compressor in order to reduce the losses.
4. To review the available flow control methods applicable in low-Reynolds-number centrifugal compressors.

The first objective is considered in **Publications I** and **II**. In **Publication I**, the loss generation was firstly studied in the impeller of a centrifugal compressor, where low Reynolds numbers were achieved by downscaling the compressor geometry. In **Publication II**, loss generation was studied in a baseline compressor where low Reynolds numbers were achieved by varying the altitude and inlet conditions to ensure that the Reynolds number losses did not depend on the variation method of the Reynolds number.

When studying loss development in the compressor, a new challenge was discovered: How to divide the losses between different causes of loss? This knowledge would enable finding out the most significant loss generation mechanisms inside the compressor. Firstly, the challenge was encountered in **Publication I** with a rough estimation, which was based on dividing the impeller outlet into subregions corresponding to different losses. Secondly, the challenge was tried to be dealt with the loss coefficients found in the literature. However, the results presented in **Publication II** indicated that the loss coefficients relying on an assumption of a uniform flow field and requiring a specification of the boundary layer edge were impractical in centrifugal compressors due to complex flow fields. As the knowledge of the boundary layer thickness inside the compressor would bring novelty to the study of loss development with varying Reynolds numbers, the second objective was set.

The second objective was considered in **Publication III**, where a hybrid method was proposed for defining the free-stream velocity and calculating the boundary layer thickness inside the blade passage of a centrifugal compressor. The first and third objectives were considered in **Publication V**, where the method presented in **Publication III** was used to

analyse the losses inside the impeller and vaneless diffuser with more a sophisticated approach than in **Publications I** and **II**. The fourth objective was considered in **Publication IV**, which was a review of the state-of-the-art of active and passive flow control methods.

1.3 Outline of the thesis

The thesis is divided into six chapters.

Chapter 1 describes the background, objectives, and outline of the thesis.

Chapter 2 describes briefly previous research concerning the effect of the Reynolds number on compressor performance.

Chapter 3 presents the numerical methods used in **Publications I–III** and **V**, a mesh independence study and validation of the numerical results.

Chapter 4 concerns **Publication III**, explaining the development of a hybrid method.

Chapters 5 and 6 present the main findings of **Publications I–V** and the conclusions based on the findings.

2 Literature review

A decrease in the Reynolds number increases the boundary layer thickness and friction losses (Schlichting, 1979). With respect to centrifugal compressors, increased boundary layer thickness and friction losses lead to deteriorated performance, i.e., lower efficiency and pressure ratio. The decrease in the Reynolds number results from a change in the compressor size, the operating conditions, or the medium (Casey, 1985). In this thesis, the Reynolds number is based on the true chord length (a distance along a straight line at mid-span from the blade leading edge to the trailing edge), relative inlet velocity and inlet flow conditions

$$Re_{\mathrm{c}} = w_1 c / \nu_1. \tag{2.1}$$

For evaluating the compressor performance, the adiabatic compression process is assumed, and the total-to-total isentropic efficiency

$$\eta_{\mathrm{s,tt}} = \frac{\left(\frac{p_{\mathrm{t3}}}{p_{\mathrm{t1}}}\right)^{\frac{R}{c_{\mathrm{p}}}} - 1}{\frac{T_{\mathrm{t3}}}{T_{\mathrm{t1}}} - 1} \tag{2.2}$$

is used. The isentropic efficiency is a feasible definition for single-stage compressors, whereas for multistage and high pressure ratio compressors, polytropic efficiency would be a better definition. The difference between isentropic and polytropic efficiencies at high pressure ratios results from the slopes of isobars in the enthalpy-entropy diagram, increasing with increased entropy:

$$\left(\frac{dh}{ds}\right)_{p\,=\,\mathrm{const}} = T. \tag{2.3}$$

Due to the slopes of the isobars, the actual compression flow work (which can be illustrated as the sum of the infinitesimal isentropic enthalpy rises) is greater than the flow work for the isentropic process (which is the same as the isentropic enthalpy rise):

$$\sum \Delta h_{\mathrm{s,i}} > \Delta h_{\mathrm{s}}. \tag{2.4}$$

In this thesis, the relative change in efficiency is a more important parameter than the absolute value of the efficiency. For averaging purposes, mass-averaging is used for stagnation properties and area-averaging for static properties, as suggested by Cumpsty and Horlock (2006).

This chapter describes how the effect of the Reynolds number can be accounted for in the compressor design process, as well as previous studies on the effect of the Reynolds number on the performance of the centrifugal compressor.

Table 2.1: Correction equations published in the literature.

Reference	Equation	
Old empirical formula (Wiesner, 1979)	$\frac{1-\eta}{1-\eta_{\mathrm{ref}}} = a + (1-a)\left[\frac{Re_{\mathrm{ref}}}{Re}\right]^n$	
Casey (1985)	$\Delta\eta = -\frac{c}{\mu_0}\Delta f$	(2.6)
Heß and Pelz (2010)	$\frac{1-\eta}{1-\eta_{\mathrm{ref}}} = (1-b) + b\left(\frac{Re_{\mathrm{ref}}}{Re}\right)^n$	(2.7)
Casey and Robinson (2011)	$\Delta\eta = -\frac{B_{\mathrm{ref}}}{f_{\mathrm{ref}}}\Delta f$	(2.8)
Dietmann and Casey (2013)	$\Delta\eta = -\frac{B_{\mathrm{ref}}}{f_{\mathrm{ref}}}\Delta f$	(2.9)
Pelz and Stonjek (2013)	$\Delta\eta = -\frac{1-\eta_{\mathrm{ref}}}{c_{\mathrm{f,ref}}}\Delta c_{\mathrm{f}}$	(2.10)

2.1 Correction equations

If the compressor size, the operating conditions, or the medium change from those of the test conditions, the performance characteristics of the compressor must be corrected to the appropriate Reynolds number (Casey, 1985). The effect of the Reynolds number on the compressor performance can be accounted for relatively easily in the design process by various correction equations.

Quoting Wiesner (1979) and Wright (1989), the earliest Reynolds number correction equations were published by Moody (1925) and Ackeret (circa 1930 according to Mühlemann, 1948). Later, several variations of this old empirical formula

$$\frac{1-\eta}{1-\eta_{\mathrm{ref}}} = a + (1-a)\left[\frac{Re_{\mathrm{ref}}}{Re}\right]^n \tag{2.5}$$

have been published, and in these variations the fraction of the Reynolds-number-independent losses a ranges from 0 to 0.5, and the Reynolds-number-ratio exponent n ranges from 0.1 to 0.5, depending on the compressor type (Casey and Robinson, 2011; Wiesner, 1979). In addition to the old empirical formula, Table 2.1 presents some of the correction equations published in the literature and Figure 2.1 illustrates the efficiency deterioration of an example compressor with a decreasing Reynolds number, based on the prediction of correction equations in Table 2.1. Besides the correction equations, the critical chord Reynolds number is normalised and sketched in Figure 2.1. Casey and Robinson (2011) have compared the flow in a compressor blade passage to that over a flat plate or in a pipe, and state that the compressor performance deteriorates strongly below the critical chord Reynolds number of approximately 200,000 due to the laminar behaviour of the boundary layers.

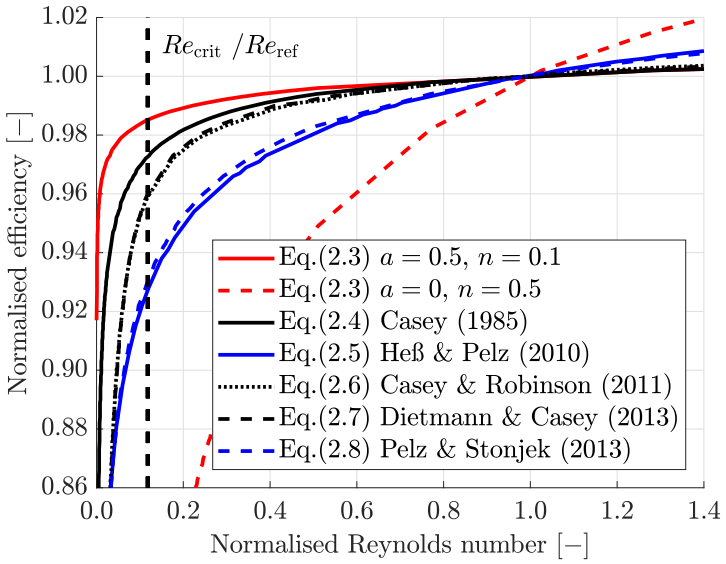

Figure 2.1: Relative change in the efficiency with a varying Reynolds number, estimated with the correction equations presented in Table 2.1. The Reynolds number was normalised by the baseline Reynolds number of the example compressor.

Figure 2.1 shows that the efficiency prediction varies significantly between the correction equations. The variation in the efficiency prediction results from the differences in the Reynolds number definition, friction factor formulation, and accounting for the Reynolds-number-independent losses. The old empirical formula (2.5) neglects the surface roughness effect and assumes that the fraction of the Reynolds-number-independent losses a is constant. As Figure 2.1 shows, the slope of the old empirical formula depends on the values of a and n, and the predictions of all the other correction equations fit between the extremes of the old empirical formula.

In the first version of Casey's (1985) correction equation (2.6), a change in the friction factor of the equivalent pipe flow due to a change in the Reynolds number causes a change in the efficiency. Unlike the old empirical formula, Casey's correction equation combines both the Reynolds number and surface roughness effects in the change in the friction factor. Casey's correction equation has been modified in 2011 (2.8) and 2013 (2.9), and in the latest version (2.9) a change in the flat plate friction factor causes a change in the efficiency. In Eqn. (2.9), the term B_{ref} refers to inefficiency due to friction losses and f_{ref} refers to the friction factor at the reference conditions. The term B_{ref} is based on experimental data from over 30 compressors ($Re_{\mathrm{c}} = 50,000 \ldots 100,000,000$), and depends on the flow coefficient as follows:

$$B_{\mathrm{ref}} = 0.05 + \frac{0.002}{\phi + 0.0025} \tag{2.11}$$

$$\phi = \frac{q_\mathrm{v}}{U_2 D_2^2}. \tag{2.12}$$

Compared to the old empirical formula, the latest version of Casey's correction equation (2.9) does not take the Reynolds-number-independent losses into account as a constant fraction but as a constant amount, because the fraction is not constant with a changing Reynolds number. The correction equation of Heß and Pelz (2.7) relates the change in efficiency to the Reynolds-dependent loss fraction b, which is a function of the flow coefficient. However, similarly to the old empirical formula, the correction equation of Heß and Pelz (2.7) neglects the effect of surface roughness. In the correction equation of Pelz and Stonjek (2.10), Reynolds-number-independent losses are not accounted for at all. Therefore, the correction equation of Pelz and Stonjek takes only frictional losses into account. In addition to frictional losses, also the Reynolds-number-independent shock, mixing, leaving, secondary kinetic energy, and tip clearance losses should be accounted for (Dietmann and Casey, 2013).

In addition to the correction equations presented in Table 2.1, the standards for compressor test procedures suggest correction equations to estimate the effect of the Reynolds number. Because the loss generation in low-Reynolds-number compressors is not well known yet, the efficiency correction equations should be used carefully. It should be noted that the correction equation presented in the standard ASME PTC 10 (1997) does not divide the losses into Reynolds-number-dependent and Reynolds-number-independent losses, and the correction equation in the standard ISO 5389 (2005) is a modification of the old empirical formula.

As indicated in this chapter, there is a wide variation between the efficiency predictions based on different Reynolds-number correction equations, and there is no agreement on the most suitable correction equation. Therefore, the most suitable correction equation is suggested below, based on the trends of numerical results accounting for the theoretical background of the correction equations presented in this chapter.

To validate the numerical results in full detail, experimental data of the flow fields inside a low-Reynolds-number compressor should be available for comparison to the flow fields inside a high-Reynolds-number compressor. Because the correction equations are based on experimental data, the numerical results are compared against the correction equations, and the correction equations are used to validate the trends of the numerical results in this thesis.

2.2 Studies on the effect of the Reynolds number

Even though the correction equations are based on empirical data, there is a limited number of experimental Reynolds number studies published in the literature. The most recent ones are summarised in Table 2.2. In the studies presented in Table 2.2, the Reynolds number is varied by changing the inlet conditions of the compressor. However, different definitions for the Reynolds number complicate the comparison of the results. The defi-

nition of the Reynolds number used by Zheng et al. (2013) is based on the impeller inlet tip diameter,

$$Re_{\mathrm{D1}} = \frac{U_1 D_1}{\nu_1}, \tag{2.13}$$

whereas the definition used by Schleer and Abhari (2005) is based on the blade height at the impeller outlet

$$Re_{\mathrm{b2}} = \frac{U_2 b_2}{\nu_1}. \tag{2.14}$$

Based on the order of magnitude of velocity components ($w_1 \approx U_1 \approx 0.5U_2$) and geometrical dimensions ($c \approx D_1 \approx 10b_2$), the following approximations are used in order to compare the cases in Table 2.2: $Re_{\mathrm{c}} \sim Re_{\mathrm{D1}}$ and $Re_{\mathrm{c}} \sim 5Re_{\mathrm{b2}}$.

Usually the design of a small-scale compressor is based on a downscaled version of a larger compressor for which the design was originally developed, and tests are conducted. Then, the performance deterioration of the downscaled compressor is estimated with the performance deterioration of the correction equations. However, the weakness of the correction equations is that they only account for the decrease in performance, but do not offer any consideration of whether the efficiency drop can be countered somehow in the design process.

When the chord Reynolds number is well above the critical one (200,000), the compressor performance does not change with the decreasing Reynolds number (Smith et al., 2015; Schleer and Abhari, 2005). In the studies of Zheng et al. (2013) and Choi et al. (2008), the Reynolds number was close to the critical one, and therefore a decrease in performance was observable. However, the numerical results of Zheng et al. (ibid.) overestimated the performance, and the predicted trend differed from the measured one.

The maximum total-to-static isentropic efficiency for a centrifugal compressor with a smooth surface, without Reynolds-number losses, and with a maximum vaned diffuser pressure recovery of 0.78 is around 84–86% (Rodgers, 1980), and small-scale centrifugal compressors operating with air as a medium and at low Reynolds numbers have 10–20 percentage points lower efficiency (Celeroton, 2018; FISCHER Engineering Solutions AG, 2017; Isomura et al., 2006; Kang et al., 2003).

To conclude, a few experimental studies on the effect of the Reynolds number have been published, but the results have not been compared to the predictions of the correction equations.

2.3 Analysis of boundary layer thickness

In order to find whether the efficiency drop can be countered in the design process of low-Reynolds-number centrifugal compressors, the loss development in centrifugal compressors with reducing Reynolds numbers must be studied. Traditionally, the loss development in centrifugal compressors has been based on loss correlations built on experimental

Table 2.2: Experimental studies on the effect of the Reynolds number.

Reference	Reynolds Number		Change in Performance
Smith et al. (2015)	$Re_\mathrm{c} = w_1 c/\nu_1$	$680,000 - 840,000$	No change
Zheng et al. (2013)	$Re_\mathrm{D1} = U_1 D_1/\nu_1$	$296,000 - 986,000$	6.9% decrease in $\eta_\mathrm{s,tt}$
Choi et al. (2008)	$Re_\mathrm{c} = w_1 c/\nu_1$	$24,000 - 244,000$	Increased losses
Schleer and Abhari (2005)	$Re_\mathrm{b2} = U_2 b_2/\nu_1$	$160,000 - 530,000$	0.5% decrease in Δp_ts

data. For example, the losses in the blade cascade boundary layers are estimated with different loss coefficients (Denton, 1993; Prust Jr., 1973), which rely on the assumption of a uniform flow field between the blades.

The boundary layer entropy loss coefficient of Denton (1993)

$$\zeta_\mathrm{bl} = 2 \sum \frac{c_\mathrm{s}}{p \cos \beta_1} \int_0^1 C_\mathrm{d} \left(\frac{w}{w_1} \right)^3 d \left(\frac{x}{c_\mathrm{s}} \right) \tag{2.15}$$

integrates entropy increase at one spanwise location over the blade surface in the meridional direction and sums the loss generation on both surfaces. The dissipation coefficient C_d is 0.002 as suggested by Denton (ibid.), the relative flow angle β_1 is defined from the axial direction, and the relative velocity w is defined at the edge of the boundary layer.

The boundary layer kinetic energy loss coefficient of Prust Jr. (1973)

$$\zeta_\mathrm{bl} = \frac{\Psi^*_\mathrm{te}}{1 - \delta^*_\mathrm{te} - t^*_\mathrm{te}} \tag{2.16}$$

integrates the kinetic energy loss at one meridional location over the blade passage in the pitchwise direction. The dimensionless energy, displacement, and trailing-edge thicknesses are defined as

$$\Psi^*_\mathrm{te} = \int_0^1 \left[1 - \left(\frac{w}{U_\infty} \right)^2 \right] \left(\frac{\rho w}{\rho_\infty U_\infty} \right) d \left(\frac{y}{p} \right) \tag{2.17}$$

$$\delta^*_\mathrm{te} = 1 - t^*_\mathrm{te} - \int_0^1 \left(\frac{\rho w}{\rho_\infty U_\infty} \right) d \left(\frac{y}{p} \right) \tag{2.18}$$

$$t^*_\mathrm{te} = \frac{t_\mathrm{te}}{p \cos \beta_\mathrm{te}}. \tag{2.19}$$

The density ratio $\rho/\rho_\infty \approx 1$ is assumed here, and according to the numerical results of

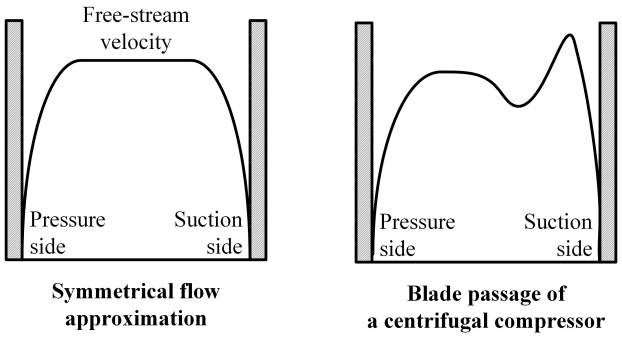

Figure 2.2: Schematic presentation of the pitchwise idealised symmetrical and typical velocity profiles of a centrifugal compressor.

this work, the assumption seems to be valid. The relative flow angle β_{te} is defined from the radial direction.

The challenge in the use of these loss coefficients is that knowledge of the relative velocity at the boundary layer edge is required, or the symmetrical flow field in the blade passage should be assumed. Analysis of the boundary layer thickness in the centrifugal compressor blade passages is difficult, as specification of the free-stream velocity is not as straightforward as in cases of flat plates or stationary blade cascades, due to the highly non-uniform flow field resulting from the jet-wake flow structure, as illustrated in Figure 2.2. In addition, the boundary layer development is not 2-dimensional in the centrifugal compressor due to the complex flow field resulting from the 3-dimensional effects.

Thus, free-stream velocity cannot be calculated with the same method as in the case of low-speed turbine cascades (Harrison, 1990; Lynch and Thole, 2016), compressor cascades (Weber et al., 2002), or one-dimensional centrifugal compressor simulation (Klausner and Gampe, 2014). In low-speed turbine cascades (Harrison, 1990), the assumption of incompressible flow made it possible to calculate local free-stream velocities from the inlet stagnation pressure and blade surface pressure. Due to the compressibility effects and a complex flow field even at the mid-span, this method is not well-suited for centrifugal compressors. Alternatively, free-stream velocity at the blade throat in one-dimensional centrifugal compressor simulation (Klausner and Gampe, 2014) was defined as an average of the blade inlet relative velocity and critical speed at the throat in order to calculate the boundary layer blockage. However, the present study concentrates on three-dimensional centrifugal compressor simulation, where the aim is to calculate the boundary layer thicknesses on the blade and endwall surfaces.

A more symmetrical total pressure distribution of the axial compressor (Weber et al., 2002) compared to that of centrifugal ones makes the definition of free-stream velocity more straightforward. Near the axial turbine endwalls, Lynch and Thole (2016) measured

the velocity profile in the spanwise direction and used the exact measured velocity at a corresponding spanwise location as free-stream velocity. This method works in blade cascades with a uniform flow field in the spanwise direction (Hergt et al., 2006), and to some extent, this might work if the boundary layers on the endwalls of a centrifugal compressor were studied, but not in the case of the blade boundary layers, due to a jet-wake flow structure. Choi et al. (2008) conclude that free-stream velocity cannot be defined in blade passages, and avoid the problem in an axial compressor by defining the boundary layer as a location from the blade surface where the velocity gradient between two adjacent data points is less than one percent.

Without being able to define the edge of a boundary layer on the blade surface or the endwall reliably, the post-processing of modelling results and comparison between different loss sources becomes user-dependent. This dependency generates challenges in a reliable comparison of different studies; e.g. in the literature (Bousquet et al., 2014; Zheng et al., 2013), conclusions about the boundary layer thicknesses in radial turbomachinery have been drawn from numerical results, even though the method for calculating the boundary layer thickness remains unclear to the reader. For example, Bousquet et al. (2014) seem to estimate the boundary layer thickness on the blade suction side based on the axial velocity distribution at the location of 2 mm downstream from the blade leading edge. Zheng et al. (2013) conclude that at the 16% lower Reynolds number, the boundary layer thickness increased mostly near the full blade leading edge, the increment being equal on both sides of the blade. Near the splitter blade and trailing edges, the increase in the boundary layer thickness was relatively small.

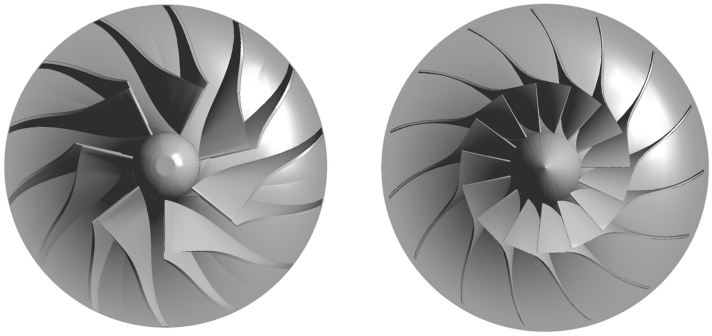

Figure 3.1: Compressor geometries (not to scale).

3 Methods and numerical model

The effect of the Reynolds number was studied numerically in two centrifugal compressors; one with splitter blades and the other without them (Figure 3.1). Both compressors were unshrouded and included a vaneless diffuser. The compressor with splitter blades was studied experimentally and numerically at Lappeenranta University of Technology, in Finland (Jaatinen-Värri et al., 2013a) and the compressor without splitter blades is the test case Radiver, in which the measurements were carried out at the Institute of Jet Propulsion and Turbomachinery at RWTH Aachen, Germany, and part of the research was funded by the Deutsche Forschungsgemeinschaft (DFG) (Ziegler et al., 2003). The compressor with splitter blades was studied at the design point (total-to-total pressure ratio around 1.8) and the compressor without splitter blades at the peak efficiency point at a reduced speed $n/n_{\mathrm{DES}} = 0.8$ (total-to-total pressure ratio around 2.5). Details of the compressor geometries and important dimensionless performance parameters at the design/peak efficiency point are shown in Table 3.1.

Both compressors were modelled at three different operating points (Table 3.2); the one with splitter blades at the design operating point, near choke and near stall, and the one without splitter blades at the peak efficiency point, near choke and near stall. The operating points near stall and choke were chosen by comparing the measured operating maps and typical values used in the literature (Shahin et al., 2017; Weber et al., 2016; Bousquet et al., 2014, 2013; Ding et al., 2013; Yang et al., 2012; Xu et al., 2011; Röyttä et al., 2009b). The near stall point does not represent the real stall point, but is the point at a low flow rate that converges stably when modelled.

The modelled operating points are shown in Figure 3.2. All the compressor performance curves were provided by Jaatinen-Värri et al. (2013b) for the compressor with splitter blades and by Ziegler et al. (2003) for the compressor without splitter blades. These three

Table 3.1: Technical data of the compressors.

	With splitter blades	Without splitter blades
Number of blades	$7+7$	15
Relative blade height ($\frac{b_2}{D_2}$)	0.058	0.041
Relative tip clearance ($\frac{t}{b_2}$)	0.052	0.045
Chord Reynolds number ($Re_{\mathrm{c,ref}} = \frac{w_1 c}{\nu_1}$)	$17 \cdot 10^5$	$16 \cdot 10^5$
Flow coefficient ($\phi = \frac{q_\mathrm{v}}{U_2 D_2^2}$)	0.065	0.051
Pressure coefficient ($\psi = \frac{\Delta h_\mathrm{s}}{U_2^2}$)	0.520	0.450
Specific speed ($N_\mathrm{s} = \frac{\omega\sqrt{q_\mathrm{v}}}{\Delta h_\mathrm{s}^{0.75}}$)	0.830	0.830
Tip speed Mach number ($Ma_\mathrm{U} = \frac{U_2}{a_1}$)	0.920	1.170

Table 3.2: Modelled operating points.

With splitter blades	$q_\mathrm{m}/q_\mathrm{m,DES}$	n/n_DES
Near stall	0.6	1.0
At the design point	1.0	1.0
Near choke	1.3	1.0
Without splitter blades	$q_\mathrm{m}/q_\mathrm{m,PE}$	n/n_DES
Near stall	0.8	0.8
At the design point	1.0	0.8
Near choke	1.2	0.8

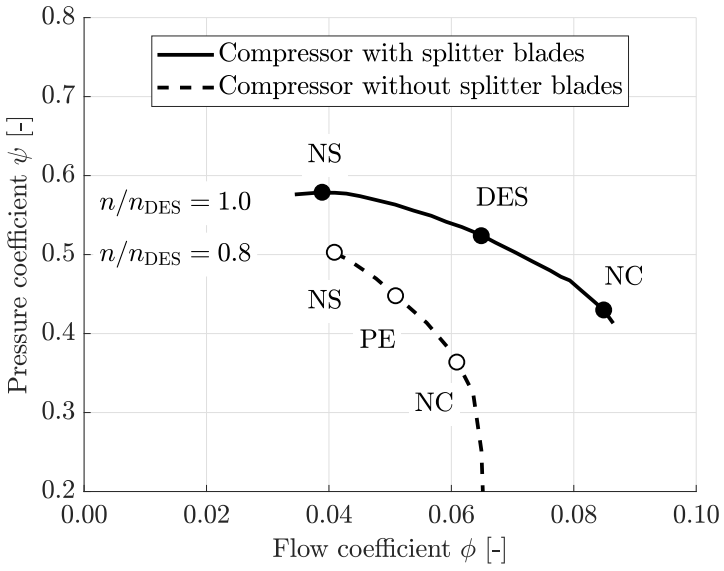

Figure 3.2: Dimensionless compressor map.

operating conditions at the baseline Reynolds number ($Re_{\mathrm{c,ref}}$ in Table 3.1) are used in order to validate the numerical results against experimental data. In addition, they are used to illustrate the difference between changing the Reynolds number and changing the operating point.

In addition to the three operating conditions at the baseline Reynolds number $Re_{\mathrm{c,ref}}$, the effect of a varying Reynolds number was studied. In **Publications I** and **V**, the Reynolds number was varied by changing the compressor size, and in **Publication II** by changing the compressor inlet conditions. When changing the compressor size, all geometric dimensions of the compressor were scaled with the same scaling factor as the impeller outlet diameter

$$SF = \frac{D_{2,\mathrm{scaled}}}{D_{2,\mathrm{baseline}}}. \tag{3.1}$$

Also, the same ideal gas properties of air were used for the downscaled compressors as for the baseline compressor. All the dimensionless numbers (flow coefficient ϕ, pressure coefficient ψ, and impeller tip speed Mach number Ma_{U}) were kept constant, except for the Reynolds number, which decreased as the compressor was downscaled. The studied chord Reynolds number varied from 1,700,000 to 80,000, with the scaling factor varying from 1 to 0.05. The downscaled compressors were modelled at the design/peak efficiency points.

When changing the inlet conditions of the compressor, the flow coefficient and impeller tip speed Mach number were kept constant, while the inlet pressure and temperature were decreased based on the properties of the standard atmosphere. To keep the compressor

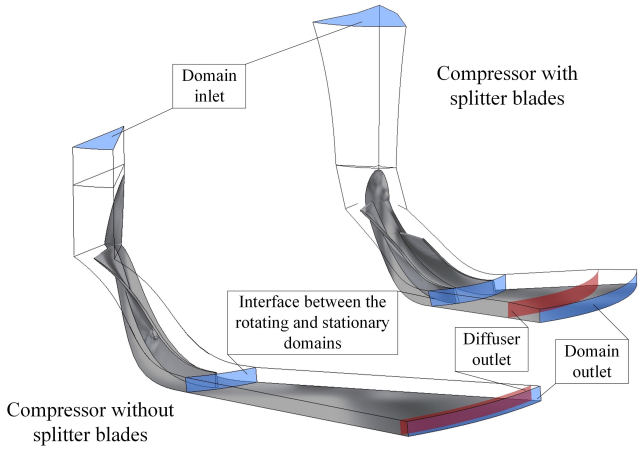

Figure 3.3: Computational domains.

operating point the same at the low chord Reynolds number of 60,000 (25 km above sea level) as at the high Reynolds number (sea level), the rotational speed and volume flow rate were decreased with respect to the change in the inlet temperature.

The commercial software ANSYS CFX 16.0/17.0 was used for steady-state numerical calculations. As rotational periodicity was assumed, the volute was neglected and the computational domain reached from the inlet section to downstream of the diffuser outlet. Due to the simplified geometry and neglect of the volute, asymmetric effects from the volute were also neglected. However, this study concentrated in more detail on the design operating condition in which the asymmetric effects are not as important as in the off-design operating conditions. The computational domains are shown in Figure 3.3.

The frozen rotor approach was used to model the transition between the rotating and stationary domains. A similar approach was used in the compressor modelling by Turunen-Saaresti et al. (2006). An alternative approach to steady-state interface modelling is a mixing plane approach in which the fluxes are circumferentially averaged. The mixing plane approach is generally used for cases with strong interaction between e.g. an impeller and vaned diffuser. However, in this study the diffuser is vaneless and therefore, the interaction with the impeller is weak compared to a vaned diffuser. According to the study of Liu and Hill (2000), the frozen rotor and mixing plane approaches gave similar results, when modelling a turbo compressor with a vaneless diffuser. In this thesis, the location of the interface between the rotating and stationary domains was $1.01r_2$ in the compressor with splitter blades and $1.03r_2$ in the compressor without splitter blades. For a comparison, Gibson et al. (2017) located the interface at $1.02r_2$.

The total pressure and total temperature were specified at the inlet boundary, and the mass flow rate at the outlet boundary, similarly as specified by Guo et al. (2007) and Smirnov

et al. (2007). The solid wall surfaces were modelled with adiabatic and no-slip conditions.

Turbulence was modelled by using the two-equation $k-\omega$ Shear Stress Transport (SST) model. The model is widely used and has been validated for turbomachinery applications (Menter, 2009). Recently, Gibson et al. (2017) used the test case Radiver to demonstrate the differences between five turbulence models. They conclude that the $k-\omega$ SST model is reasonably robust to predict the basic local flow phenomena in the centrifugal compressor. The values of the non-dimensional wall distance were below unity on most of the surfaces, with the most challenging region for meshing being the stagnation point at the blade leading edge. At the inlet of the computational domain, the turbulence intensity of 5% was specified similarly as by Smirnov et al. (2007).

The target values for numerical convergence were the efficiency and mass imbalance between the inlet and outlet. Convergence was achieved when the change in the target values was below 0.1% and the change in the normalised residuals of energy, mass, momentum, and turbulence parameters was stabilised.

3.1 Mesh independence study

For the mesh independence study, three structured meshes with 0.8, 1.9, and 4.3 million computational cells were used for the compressor with splitter blades, and three meshes with 0.7, 1.7, and 3.8 million cells for the compressor without splitter blades. As a result of the mesh independence study (Figure 3.4), the meshes with 1.9 and 1.7 million cells were chosen for the compressors with and without splitter blades, respectively (Figure 3.5). The target values regarding mesh independence were the total-to-total isentropic efficiency and total-to-total pressure ratio between the computational domain inlet and diffuser outlet. The meshes of the baseline compressors were scaled for the downscaled compressors, i.e. so that they had the same number of cells in both the baseline and the downscaled cases.

To reduce the discretisation error, the mesh was made denser in the areas of larger gradients, and the high resolution discretisation scheme was used. The discretisation error was estimated by using the procedure presented by Celik et al. (2008). The estimated discretisation error; i.e. the fine-grid convergence index $\mathrm{GCI}_{\mathrm{fine}}$ is shown with error bars in Figure 3.4, which presents the results of the mesh independence study for the compressors with splitter blades (top) and without splitter blades (bottom). The fine-grid convergence index with the apparent order of convergence p is shown in Table 3.3.

The apparent order of convergence is proportional to the order of the discretisation scheme, and according to the ASME standard (Coleman, 2009), the apparent order of convergence should be limited to value of two referring to the high resolution discretisation scheme. For the fine-grid convergence index presented in Figure 3.4, the apparent order of convergence p is limited to two, but the obtained values are shown in Table 3.3. If the apparent order of convergence were not limited to two, the discretisation error would be under-

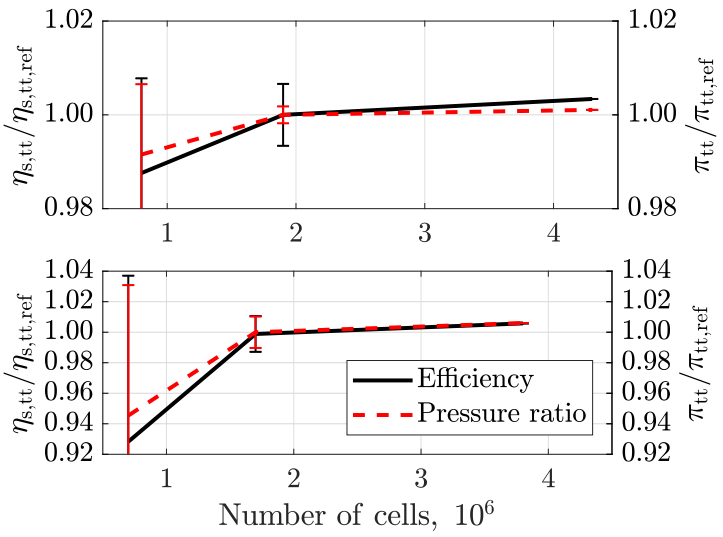

Figure 3.4: Mesh independence of the compressors with splitter blades (upper) and without splitter blades (lower). The bars present the discretisation error.

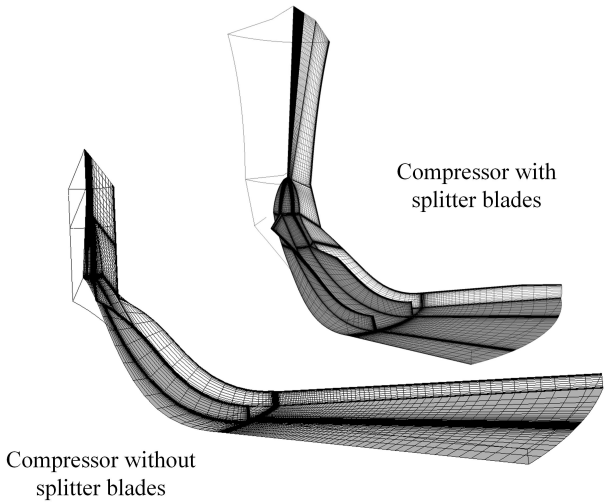

Figure 3.5: Structured meshes of the compressors with and without splitter blades with 1.9 and 1.7 million cells, respectively.

Table 3.3: Discretisation error presented with the fine-grid convergence index $\mathrm{GCI}_{\mathrm{fine}}$ (in the calculation, p limited to 2) and apparent order of convergence p.

	$\eta_{\mathrm{s,tt}}$		π_{tt}	
	$\mathrm{GCI}_{\mathrm{fine}}$	p	$\mathrm{GCI}_{\mathrm{fine}}$	p
With splitter blades	0.66%	4.13	0.18%	7.84
Without splitter blades	1.17%	8.22	1.03%	7.26

estimated. The obtained values of p differ from the high-resolution scheme value of two because the observed values of efficiency and pressure ratio are very close to each other between the two finest meshes, and therefore the procedure for the calculation of p does not work properly (Celik et al., 2008).

3.2 Validation against experimental data

The numerical results for the baseline, non-scaled compressors were compared to the experimental results. The computational and measured total-to-total pressure ratios and efficiencies are shown as functions of the normalised mass flow rate in Figure 3.6. The efficiency and pressure ratio were normalised by the measured value at the design/peak efficiency point, and the mass flow rate was normalised by the design/peak efficiency mass flow rate. For computational results, the discretisation error is presented in Figure 3.6.

The validation of the numerical model shows an over-prediction of the efficiency and pressure ratio in both cases, but still the trend is captured. It must be noted that the computational efficiency and pressure ratio were calculated between the computational domain inlet and diffuser outlet, whereas the measurements were conducted between the compressor inlet and outlet for both compressors. Therefore, the computational results do not account for the pressure loss in the volute or in the exit cone, which can be seen as part of the difference between the computational and measured values. For the test case Radiver (the compressor without splitter blades), the data at the vaneless diffuser outlet is not available, because the probe measurement conducted only at one circumferential position does not represent the averaged flow at the diffuser outlet due to the asymmetric effects from the downstream compressor housing (Ziegler, 2003).

To give an estimation of the additional losses due to the volute and exit cone, the experimental results of Hagelstein et al. (2000) for the total pressure loss coefficient of $0.4-0.85$ were used in the compressors studied in this work. This estimation resulted in $1.5-6\%$ of additional losses in the total-to-total pressure ratio and total-to-total isentropic efficiency due to the volute and the exit cone. The measured total pressure drop of approximately 6 kPa (total pressure loss coefficient of approximately 0.5) in the compressor with splitter blades at the design point resulted in 4% of additional losses, which is of the same order

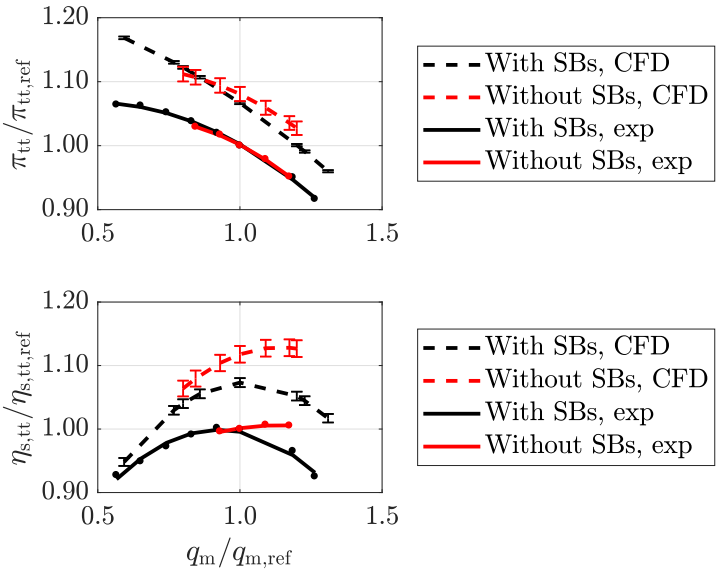

Figure 3.6: Validation of computational results of pressure ratio (upper) and efficiency (lower) against experimental data.

of magnitude as the losses presented by Hagelstein et al. (2000).

The losses due to disk friction, leakage flow through the backside cavity, or surface roughness were also neglected in the computational model. According to Sun et al. (2009), leakage through the backside cavity can be responsible for approximately 1% of additional losses in the pressure ratio and efficiency. Part of the difference between the computational and measured results was also due to the weakness of the two-equation models in predicting all the losses in a complex flow field of the centrifugal compressor (Wilcox, 1994).

Despite the over-prediction of the efficiency and the pressure ratio, the computational model predicted the area-averaged values of the absolute velocity, relative velocity and flow angle well. These parameters from the computational model are compared to the measured ones in Figure 3.7. The relative differences between the area-averaged measured and modelled values of the absolute velocity, relative velocity and flow angle (from the radial direction) in the compressor without splitter blades at $r/r_2 = 0.99$ were -2.5%, -1.7% and +1.0%, respectively. A similar numerical approach as used in this thesis was used by Bareiß et al. (2015), and the comparison of their numerical results against the experimental ones showed that the model over-predicted the total-to-total pressure ratio by 7.4% and the total-to-total isentropic efficiency by 8.9% at the design point, the values being similar as in this thesis.

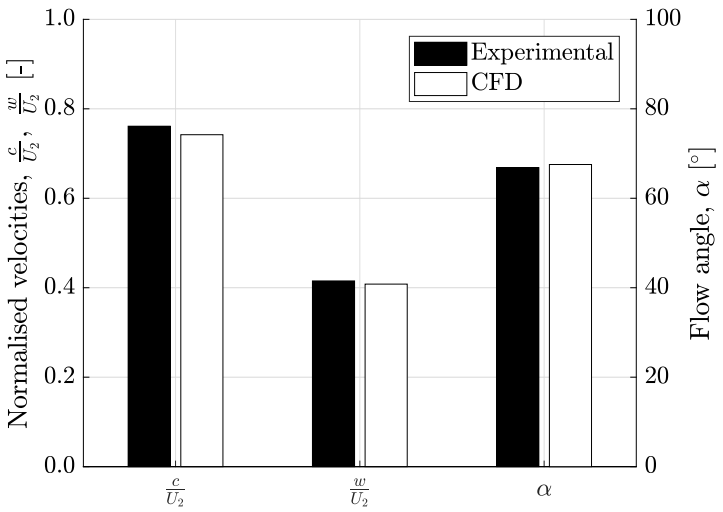

Figure 3.7: Validation of computational results of normalised absolute velocity, normalised relative velocity, and flow angle (from the radial direction) in the compressor without splitter blades at $r/r_2 = 0.99$ against experimental data.

4 Development of the hybrid method

Getting detailed information about the loss development with the decreasing Reynolds number requires knowledge about the boundary layer losses near the blade surfaces and endwalls, losses associated with the tip clearance, and secondary losses concentrated in the wake.

The differentiation of losses originating from different causes is challenging in centrifugal compressors, but in many compressors the blade boundary layer, endwall boundary layer and tip leakage losses are of the same order of magnitude (Denton, 1993). Despite the complexity, the differentiation of losses would bring novelty to the low-Reynolds-number studies, as it would give information about the most potential loss development mechanisms to be reduced in the compressor in order to improve its performance.

In the beginning of this study, the loss differentiation was based on a qualitative approach for separating different loss development mechanisms from each other. The impeller outlet area was divided into smaller subregions, which roughly covered the tip clearance, blade and hub boundary layers, and the wake (**Publications I** and **II**). The idea about the subregions arose from the study of Biester et al. (2013), where the entropy generation due to labyrinth leakage in the axial turbine was integrated in small subregions separated from each other in the computational domain. The increase in the specific entropy from the impeller inlet to the subregions at the impeller outlet was calculated, and conclusions about the fraction of separate losses from the total losses were drawn. However, this method suffered from a lack of the knowledge about the location of the boundary layer edge.

The method based on subregions was used in **Publications I** and **II**, and the subregions were defined as follows:

1. Losses associated with the tip clearance: rectangular plane in the tip clearance
2. Losses concentrated in the wake: area of low meridional velocity
3. Boundary layer losses: area of low meridional velocity near the blade and hub surfaces (wake area excluded from the impeller outlet area)

The definition of the wake as a low-meridional-velocity area on the blade suction side ($c_\mathrm{m}/U_2 \leq 0.2$) was similar to that in the study of Eckardt (1976). As the specification of the boundary layer edge in a highly non-uniform flow field is challenging, the boundary layers were separated from the low-meridional-velocity area ($c_\mathrm{m}/U_2 \leq 0.2$) at the impeller outlet by excluding the wake area. The definitions presented above led to a rough estimation of the loss distribution, which anyway indicates somehow the fraction of separate losses that are difficult to distinguish from each others due to cross-coupling.

To analyse the amount of losses developed by different mechanisms, the change in the specific entropy was used as a measure of losses, as the change of entropy determines the performance of an adiabatic turbomachine (Denton, 1993). The results obtained with this method indicated that in the low-Reynolds-number compressor, the tip leakage and blade

boundary layer losses increase relatively more than the hub boundary layer losses or the secondary losses concentrated in the wake.

After the method based on subregions, the applicability of the loss coefficients was studied in the highly non-uniform centrifugal compressor flow field. The loss coefficients of Denton (1993) and Prust Jr. (1973) were chosen for this study. The results presented in **Publication II** indicate that the loss coefficients cannot be utilised in centrifugal compressors because they are developed for uniform flow fields between the blades and are highly sensitive to the value of velocity at the boundary layer edge. When even the calculation of the boundary layer thickness in the centrifugal compressor blade passage is difficult, the value of velocity at the boundary layer edge results in uncertainty in the loss coefficients.

As the loss coefficients failed to predict the losses in a complex flow field, and because of the lack of a unified definition of free-stream velocity in the blade passage of a centrifugal compressor, a method for calculating the boundary layer thickness in the centrifugal compressor was developed in **Publication III**. During the development of the method, different free-stream velocity definitions were compared and their effect on the boundary layer thickness were demonstrated. The demonstration indicated that the most promising free-stream velocity definition is similar to what Choi et al. (2008) used in an axial compressor study; the velocity gradient on a data line normal to the surface under investigation is calculated, and the boundary layer thickness is the distance between the surface and the location where the velocity is 99.5% of the velocity of the adjacent data point:

$$\frac{dU}{dn} = 0.005 \tag{4.1}$$

$$\Rightarrow U_{\mathrm{n}-1} = 0.995U_{\mathrm{n}}. \tag{4.2}$$

Hence, the free-stream velocity equals the velocity of the data point next to the boundary layer edge and varies along the meridional location $U_\infty = U_{\mathrm{n}}$.

In a complex centrifugal compressor flow field, the advantage of this definition of free-stream velocity is that it captures the boundary layer edge between the blade surface and the wake, but a weakness is that it does not capture the boundary layer separation. Therefore, another definition was developed for separated flow:

$$U_\delta = 0.995U_{\infty,\mathrm{ave}} \tag{4.3}$$

$$U_{\infty,\mathrm{ave}} = \frac{1}{N}\sum_{1}^{N} U_{\mathrm{n}}, \tag{4.4}$$

where U_{n} is evaluated based on an assumption of attached flow.

The combination of these two free-stream velocity definitions resulted in the hybrid method, which is able to capture both the boundary layer separation and the boundary layer edge lying between the blade surface and the wake in the complex flow field. A schematic

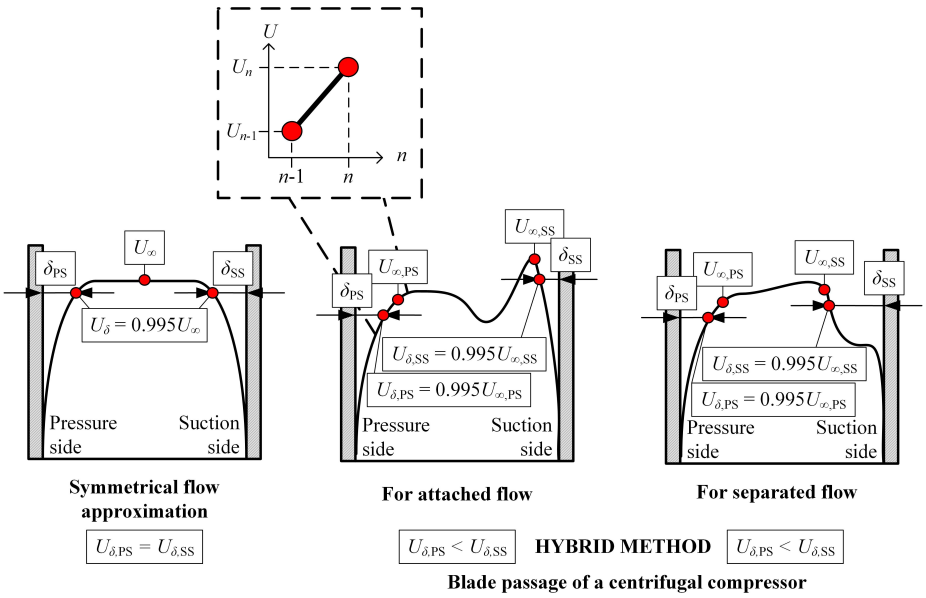

Figure 4.1: Schematic presentation of the hybrid method. Left: comparison to the pitchwise idealised symmetrical velocity profile. Middle: hybrid method for attached flow calculated with Eqn. (4.1). Right: hybrid method for separated flow calculated with Eqn. (4.3).

presentation of the hybrid method is shown in Figure 4.1, and the iterative calculation procedure for an arbitrary number of meridional locations specified by the user is as follows:

1. The flow is assumed attached: the free-stream velocity and boundary layer thickness are calculated by using Eqn. (4.1).
2. The average value for the free-stream velocity is calculated by using Eqn. (4.4).
3. The velocity profile is plotted and flow separation on the blade suction side near the leading edge is analysed qualitatively from the plot by the user.
4. The locations of flow separation are specified by the user.
5. The free-stream velocity and boundary layer thickness are calculated for the separated flow by using Eqn. (4.3).

The hybrid method enables also the calculation of the loss coefficients. However, the results in **Publication III** indicate that when the loss coefficients are based on the velocity ratio (Denton, 1993; Prust Jr., 1973), they cannot be used to compare different operating conditions resulting from a change in the mass flow rate. As the velocity ratio in Eqns. (2.15) and (2.16) dominates the value of the loss coefficients, the loss coefficients are incorrectly reduced at off-design operating conditions.

5 Loss generation in low-Reynolds-number centrifugal compressors

This chapter presents the main findings of **Publications I–V**. The main findings are based on a comparison between the baseline chord Reynolds number ($Re_{\mathrm{c,ref}} = 1,600,000/1,700,000$) and the $90 - 96\%$ lower chord Reynolds numbers ($Re_{\mathrm{c}} = 60,000 \ldots 170,000$) which are below the critical chord Reynolds number (Re_{crit}) of $200,000$.

In **Publications I** and **II**, the loss generation study was restricted to the impeller, and the loss generation mechanisms were divided into boundary layer losses, losses associated with the tip clearance, and losses concentrated in the wake. As the estimation of the boundary layer losses became more sophisticated by means of the hybrid method (**Publication III** and Chapter 4), the loss generation mechanisms under investigation were the boundary layer losses and the losses associated with the tip clearance in **Publication V**, in which both the impeller and vaneless diffuser were studied.

In addition to the boundary layer and tip clearance losses, the performance deterioration due to the low Reynolds numbers was analysed by means of blockage, blade loading, total pressure loss coefficient, pressure recovery coefficient, and total-to-total isentropic efficiency.

5.1 Boundary layer losses

The hybrid method enables the analysis of the boundary layer thickness distribution near the blade and endwall surfaces of the centrifugal compressor. The blade and endwall boundary layer thicknesses were calculated at the chosen locations along the meridional direction shown in Figures 5.1 and 5.2. In the impeller, a decrease in relative velocity causes boundary layer growth (Denton, 1993). Therefore, to calculate the blade boundary layer thickness, relative velocity values of 10,000 evenly distributed data points in the pitchwise direction were analysed at the mid-span in order to exclude the effect of the endwall boundary layers.

The number of data points was based on the sensitivity analysis presented in **Publication III**, and it corresponds to approximately 140 data points per millimeter in the compressor with splitter blades, and 180 data points per millimeter in the compressor without splitter blades at the impeller trailing edge. As stated in **Publication III**, the sensitivity of the hybrid method to the number of data points would not require as many data points for the analysis of the blade boundary layer thickness as used in this study, but due to the small increase in the boundary layer thickness with the decreasing number of data points, the number of data points of 10,000 was selected. However, the decrease in the calculated blade boundary layer thickness was only 0.5 mm maximum when the number of data points was increased from 9 to 180 per millimeter on the blade suction side of the compressor without splitter blades. The blade boundary layers occupy approximately 3%

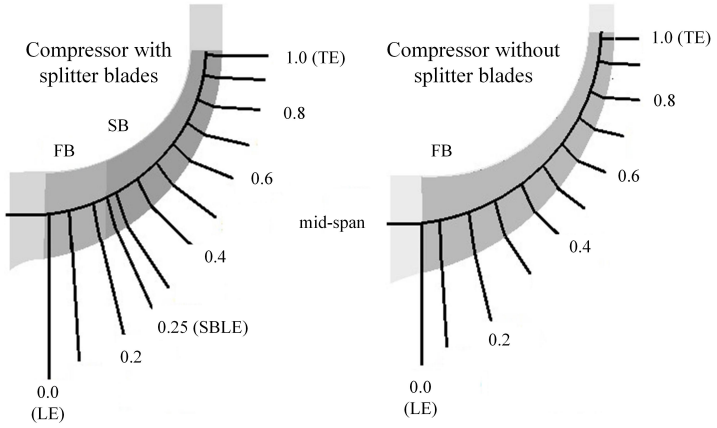

Figure 5.1: Observation planes of the blade boundary layer thickness along the meridional direction from the full blade (FB) leading edge (LE) to the trailing edge (TE).

of the passage width in the baseline case at the impeller trailing edge (passage width at the impeller trailing edge is approximately 74 mm in the baseline compressor with splitter blades and 58 mm in the baseline compressor without splitter blades).

According to the sensitivity analysis, the hybrid method was less sensitive to the number of data points in the spanwise direction than in the pitchwise direction. Therefore, relative velocity values of 160 evenly distributed data points in the impeller, and absolute velocity values of 100 evenly distributed data points in the diffuser were analysed. The velocity values were averaged in the pitchwise direction based on ten investigated locations, and the endwall boundary layer thickness was calculated from the spanwise distribution. The number of data points corresponded to approximately 5–15 points per millimeter at the impeller trailing edge, depending on the compressor. Especially in the diffuser, the sensitivity analysis and comparison of the calculated endwall boundary layer thicknesses to the velocity contours and distributions indicated that less data points were required due to the thicker endwall boundary layer thickness and more uniform velocity distribution, compared to the impeller.

To compare the blade and endwall boundary layer thicknesses between the baseline and low-Reynolds-number cases, an average of the relative change in the boundary layer thicknesses at different locations along the meridional direction was calculated, and to compare the blade boundary layer thicknesses, they were summed ($\delta_{\mathrm{FBPS}} + \delta_{\mathrm{FBSS}} + \delta_{\mathrm{SBPS}} + \delta_{\mathrm{SBSS}}$) and normalised via the pitchwise length of the modelled compressor blade passage at the impeller outlet. The relative increase in the average blade and endwall boundary layer thicknesses with the decreasing Reynolds number are shown in Table 5.1, in which the decrease in the Reynolds numbers of 90% and 95% corresponds to the cases in which the Reynolds number was varied by downscaling the baseline compressor geom-

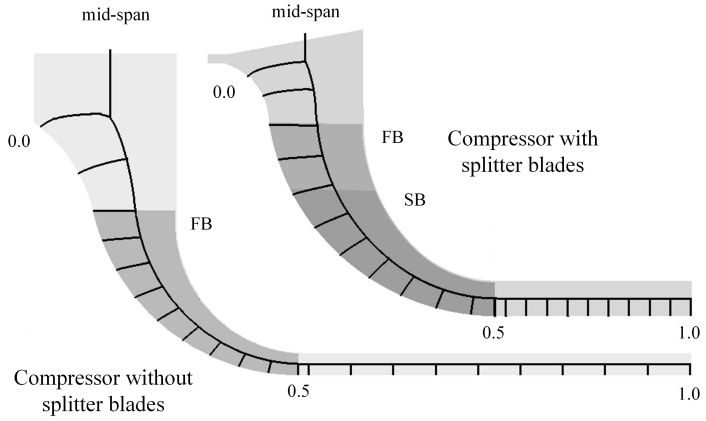

Figure 5.2: Observation planes of the endwall boundary layer thickness along the meridional direction from the impeller inlet (0.0) to the diffuser outlet (1.0).

Table 5.1: Relative increase on the average blade and endwall boundary layer thicknesses with the decreasing chord Reynolds number compared to the case with the baseline chord Reynolds number.

	$\Delta Re/Re_{\mathrm{c,ref}}$			
With splitter blades	-90%	-92%	-95%	-96%
Blade surfaces	$+22\%$	$+30\%$	$+36\%$	$+50\%$
Endwall average	$+42\%$	$+55\%$	$+62\%$	$+75\%$
Impeller average	$+30\%$	$+50\%$	$+54\%$	$+57\%$
Impeller shroud	$+34\%$	$+50\%$	$+54\%$	$+57\%$
Impeller hub	$+26\%$	$+50\%$	$+54\%$	$+57\%$
Diffuser average	$+54\%$	$+60\%$	$+69\%$	$+92\%$
Diffuser shroud	$+17\%$	$+23\%$	$+29\%$	$+42\%$
Diffuser hub	$+91\%$	$+97\%$	$+108\%$	$+142\%$
Without splitter blades	-90%	-92%	-95%	-96%
Blade surfaces	$+19\%$	$+26\%$	$+30\%$	$+40\%$
Endwall average	$+35\%$	$+38\%$	$+45\%$	$+49\%$
Impeller average	$+24\%$	$+26\%$	$+35\%$	$+41\%$
Impeller shroud	$+15\%$	$+14\%$	$+21\%$	$+22\%$
Impeller hub	$+33\%$	$+38\%$	$+48\%$	$+60\%$
Diffuser average	$+45\%$	$+49\%$	$+55\%$	$+57\%$
Diffuser shroud	$+57\%$	$+59\%$	$+59\%$	$+59\%$
Diffuser hub	$+33\%$	$+39\%$	$+50\%$	$+55\%$

etry with the scaling factors of 0.1 and 0.05, respectively. The decrease in the Reynolds numbers of 92% and 96% correspond to the cases in which the Reynolds number was varied by changing the compressor inlet conditions referring to the altitudes of 20,000 m and 25,000 m above the sea level, respectively.

Comparison of the results in Table 5.1 indicates on average greater thickening of the boundary layer near the endwalls than near the blade surfaces. In both compressors, the boundary layer thickness increased on average more in the diffuser than in the impeller. The greater thickening of the boundary layer near the impeller hub than that near the blade surfaces might result from the secondary flow which shifts the low-momentum fluid towards the impeller hub and further along the blade surfaces to the wake located in the shroud suction side corner of the blade passage (Eckardt, 1976). In the diffuser, the low-momentum fluid from the boundary layers is not shifted to the wake as it is in the impeller, resulting in greater thickening of the boundary layers.

A more detailed study of the relative increase in the boundary layer thickness indicated that the endwall boundary layer thickness increased more at the impeller hub than at the impeller shroud in the compressor without splitter blades, whereas in the compressor with splitter blades, the increase was almost equal at the impeller hub and shroud. The reason for the greater increase of the boundary layer thickness at the impeller shroud in the compressor with splitter blades might be a larger relative tip clearance than in the compressor without splitter blades.

The results in Table 5.1 indicate on average that the diffuser hub boundary layer thickness doubles with the decreasing Reynolds number in the compressor with splitter blades. The thickening of the diffuser hub boundary layer at low Reynolds numbers is illustrated in Figure 5.3, which presents the velocity distribution at the diffuser outlet ($r_3/r_2 = 1.68$) of the compressor with splitter blades. At low Reynolds numbers, the flow field becomes less uniform than at the baseline Reynolds number, as the low-momentum fluid accumulates near the diffuser hub, and the boundary layer reaches the mid-span of the diffuser passage.

Contrary to the diffuser hub boundary layer thickness, the averaged diffuser shroud boundary layer thickness in the compressor without splitter blades does not increase with the decreasing Reynolds number. The reason for the almost equal thicknesses of the normalised boundary layers is the similar velocity field at all the low Reynolds numbers, as shown in Figure 5.4, which presents the velocity distribution at the diffuser outlet ($r_3/r_2 = 2.48$) of the compressor without splitter blades.

An increase in the boundary layer thickness results in increased blockage, which is observed as an increased radial velocity. The effect of blockage on the flow field is shown in Table 5.2, in which the average increase in the radial velocity is shown with the decreasing Reynolds number. The radial velocity is calculated from the mass flow rate through the computational domain, pitchwise-averaged density distribution from the numerical

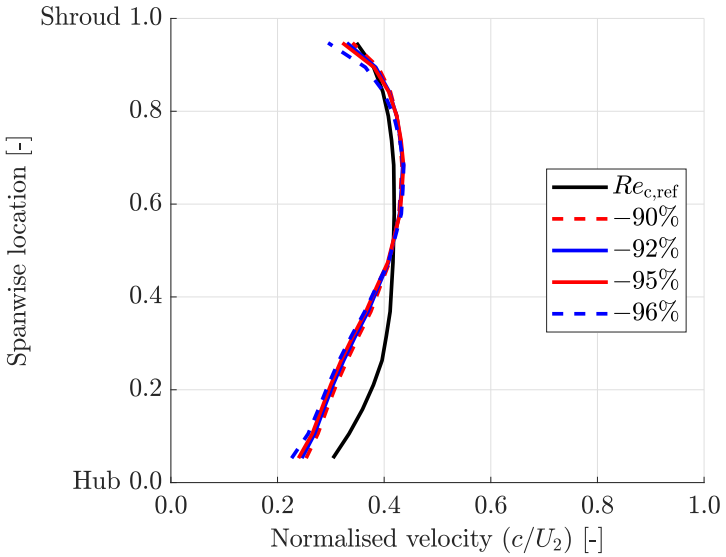

Figure 5.3: Pitchwise-averaged velocity normalised by the impeller tip speed at the diffuser outlet ($r_3/r_2 = 1.68$) of the compressor with splitter blades.

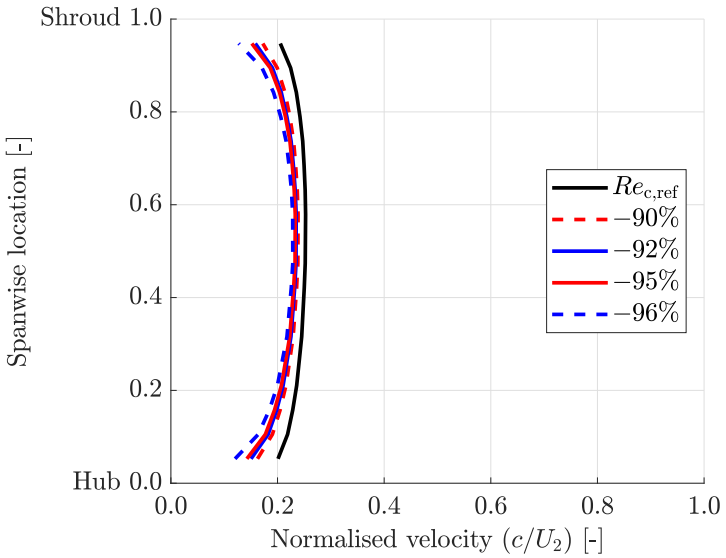

Figure 5.4: Pitchwise-averaged velocity normalised by the impeller tip speed at the diffuser outlet ($r_3/r_2 = 2.48$) of the compressor without splitter blades.

Table 5.2: Relative average increase in the radial velocity normalised by the impeller tip speed with the decreasing chord Reynolds number at the diffuser inlet ($r/r_2 = 1.04$), compared to the case with the baseline chord Reynolds number.

	-90%	-92%	-95%	-96%
With splitter blades	$+3.3\%$	$+4.2\%$	$+5.1\%$	$+6.7\%$
Without splitter blades	$+4.8\%$	$+6.4\%$	$+7.1\%$	$+10.1\%$

Table 5.3: Relative decrease in the blade loading with the decreasing chord Reynolds number compared to a case with the baseline chord Reynolds number.

	-90%	-92%	-95%	-96%
With splitter blades	-11%	-7%	-11%	-24%
Without splitter blades	-7%	-4%	-9%	-11%

simulation, and cross-sectional area of the computational domain as follows:

$$c_{\mathrm{r}} = \frac{q_{\mathrm{m,domain}}}{\rho A_{\mathrm{domain}}}. \tag{5.1}$$

The normalised radial velocity is averaged in the spanwise direction in order to calculate the relative increase. The increased radial velocity increases the wall shear stress and decreases the static pressure, resulting in greater friction losses and weaker compressor performance. These results indicate that the most potential way to decrease the losses due to low Reynolds numbers would be the control of the boundary layers near the impeller hub and diffuser surfaces. The result of the significant role of the diffuser in performance deterioration is in contrast to previous knowledge, i.e. most of the losses occur in the impeller due to the high flow velocities (Dietmann and Casey, 2013).

5.2 Tip leakage losses

In the literature, changes in the blade loading (Denton, 1993) and tangential velocity component (Jansen, 1967) have been used to estimate the change in the tip leakage losses. However, the losses associated with the tip clearance are difficult to distinguish from the endwall losses on the shroud surface, due to the tip leakage flow near the impeller shroud.

The blade loading can be presented in terms of the relative velocity difference between the blade pressure and suction surfaces, and the mean value of the relative velocities on

the blade pressure and suction surfaces (Japikse, 1996):

$$\frac{\Delta w}{w_{\mathrm{ave}}} = \frac{w_{\mathrm{SS}} - w_{\mathrm{PS}}}{\frac{1}{2}\left(w_{\mathrm{SS}} + w_{\mathrm{PS}}\right)}. \tag{5.2}$$

The change in the blade loading with the decreasing Reynolds number is presented in Table 5.3. In the compressor with splitter blades, the blade loading has been calculated separately for the full and splitter blades, and the value in Table 5.3 is an average between the blades. The values of the relative velocities have been calculated at the boundary layer edge at the mid-span in order to exclude the effect of the endwall boundary layers. The deterioration of the blade loading at mid-span means that the difference between the relative velocities on the blade pressure and suction sides decreases and

$$\frac{w_{\mathrm{PS}}}{w_{\mathrm{SS}}} \to 1. \tag{5.3}$$

The effect of the deteriorated blade loading on the tip leakage can be analysed by means of tip leakage loss coefficients. Denton (1993) presents the following tip leakage entropy loss coefficient for incompressible, two-dimensional flow in a turbomachine cascade:

$$\zeta_{\mathrm{tl}} = \frac{2C_{\mathrm{d}}tc}{bp\cos\beta_2}\int_0^1 \left(\frac{w_{\mathrm{SS}}}{w_2}\right)^3 \left(1 - \frac{w_{\mathrm{PS}}}{w_{\mathrm{SS}}}\right)\sqrt{\left[1 - \left(\frac{w_{\mathrm{PS}}}{w_{\mathrm{SS}}}\right)^2\right]}\, d\left(\frac{x}{c}\right). \tag{5.4}$$

The substitution of Eqn. (5.3) into the tip leakage entropy loss coefficient results in a decreased tip leakage loss with the decreased blade loading and Reynolds number:

$$\zeta_{\mathrm{tl}} \to 0. \tag{5.5}$$

For comparison, the results published by Choi et al. (2008) indicate a reduction in the tip leakage loss with the decreasing Reynolds number in an axial compressor, in which the tip leakage loss based on Eqn. (5.4) reduced by 26% when the Reynolds number decreased from $244,000$ to $24,400$.

Jansen (1967) presents the following tip leakage loss coefficient for a centrifugal impeller:

$$\zeta_{\mathrm{tl}} = 0.6\left(\frac{t}{b_2}\right)\left(\frac{c_{\mathrm{u},2}}{U_2}\right)\sqrt{\frac{4\pi}{b_2 Z}\left[\frac{r_{\mathrm{s},1}^2 - r_{\mathrm{h},1}^2}{(r_2 - r_{\mathrm{s},1})\left(1 + \frac{\rho_2}{\rho_1}\right)}\right]\left(\frac{c_{\mathrm{u},2}}{U_2}\right)\left(\frac{c_1}{U_1}\right)}. \tag{5.6}$$

In the tip leakage loss coefficient of Jansen (1967), a decrease in the tangential velocity component at the impeller outlet results in a lower loss coefficient. At the 96% lower chord Reynolds number than the baseline Reynolds number, the mass-flow averaged tan-

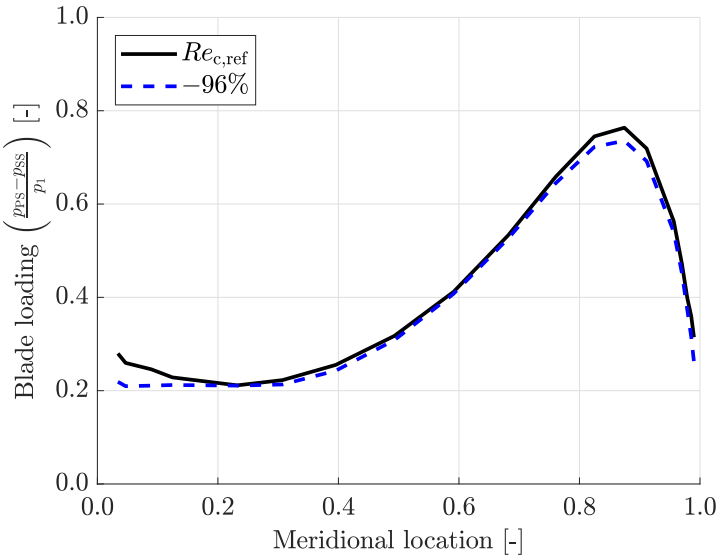

Figure 5.5: Blade loading defined as a normalised pressure difference across the blade at the mid-span of the compressor without splitter blades.

gential velocity component normalised by the impeller tip speed decreased by 1% at the impeller outlet of the compressor with splitter blades and by 2% at the impeller outlet of the other compressor, indicating a decrease in the tip leakage loss coefficient of Jansen (1967). However, the mass-flow-averaged tangential velocity component included the effect of relatively thicker boundary layers, and therefore the effect of the tip leakage is difficult to distinguish from the boundary layer losses.

On the other hand, the blade loading can be defined as a pressure difference across the blade (Yamada et al., 2010). In Figures 5.5 and 5.6, the pressure difference across the blade is normalised by the pressure at the compressor inlet as follows:

$$\frac{p_{\mathrm{PS}} - p_{\mathrm{SS}}}{p_1}. \tag{5.7}$$

At the mid-span (Figure 5.5), the blade loading based on Eqn. (5.7) decreased at the 96% lower Reynolds number by 6% on average, which corresponds to the 11% decrease in the blade loading based on Eqn. (5.2) and presented in Table 5.3. Near the shroud, at the 95% span (Figure 5.6), the blade loading based on Eqn. (5.7) increased by 10% with the decreased Reynolds number. As the pressure difference across the blade drives the tip leakage flow from the pressure side to the suction side, and the increased blade loading corresponds to the strengthened tip leakage flow (Denton, 1993; Vogel et al., 2015), the results presented in Figure 5.6 indicate that the tip leakage was strengthened with the decreased Reynolds number.

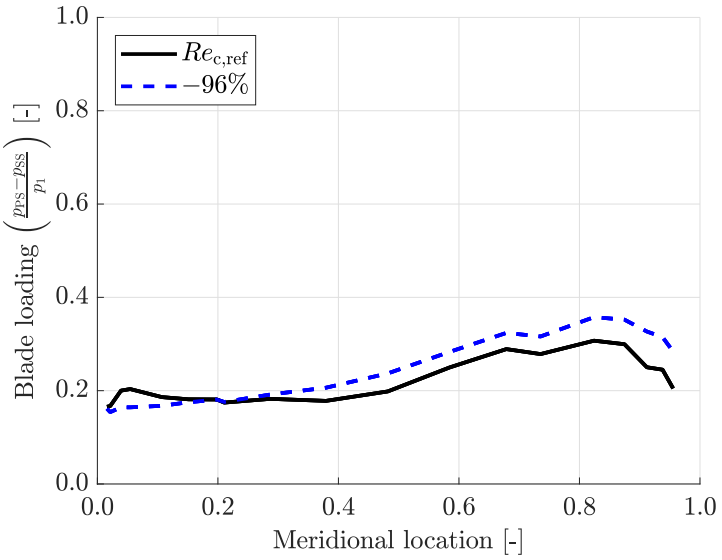

Figure 5.6: Blade loading defined as a normalised pressure difference across the blade at the 95% span of the compressor without splitter blades.

In conclusion, a distinction between tip leakage and shroud boundary layer losses is difficult to make, but the blade loading based on the pressure difference across the blade near the shroud indicated a strengthening of the tip leakage flow with the decreased Reynolds number when the relative tip clearance remained constant. In the micro-scale centrifugal compressors, the relatively larger tip clearances due to the manufacturing and controlling reasons would result in further increased tip leakage losses. The numerical results of this work indicated that a 100% larger relative tip clearance (from 25 μm to 50 μm) in the compressor without splitter blades at the 95% lower Reynolds number than the baseline one resulted in a less than 1% additional decrease in the efficiency. This result agrees with the results presented elsewhere (Turunen-Saaresti and Jaatinen, 2013).

5.3 Performance deterioration

The increased friction losses with the decreasing Reynolds number due to the thicker boundary layer result in deteriorated compressor performance. The deteriorated performance can be observed e.g. as an increased total pressure loss coefficient and decreased pressure recovery coefficient in the diffuser, and decreased total-to-total isentropic efficiency in the compressor stage. The changes in the total pressure loss coefficient

$$K_{\mathrm{p}} = \frac{p_{\mathrm{t},2} - p_{\mathrm{t},3}}{p_{\mathrm{t},2} - p_{\mathrm{s},2}} \tag{5.8}$$

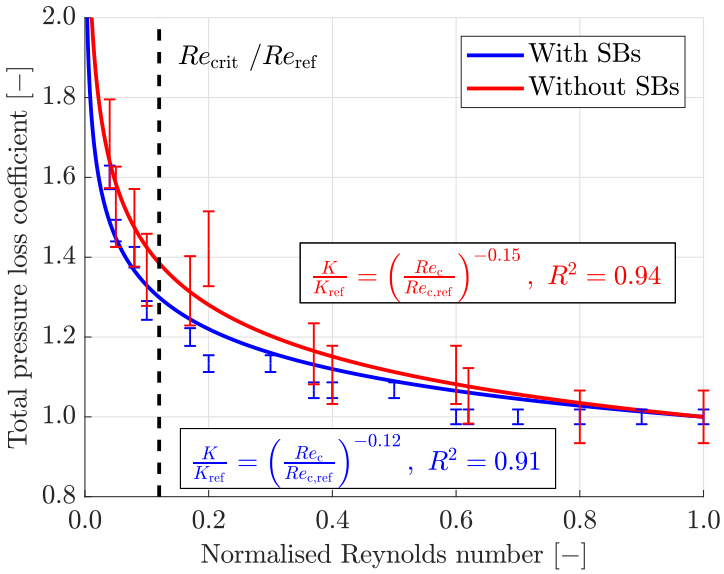

Figure 5.7: Change in a normalised total pressure loss coefficient with a varying Reynolds number. $R^2 = 0.91$ with splitter blades (SBs) and $R^2 = 0.94$ without splitter blades.

and pressure recovery coefficient

$$C_{\mathrm{pr}} = \frac{p_{\mathrm{s},3} - p_{\mathrm{s},2}}{p_{\mathrm{t},2} - p_{\mathrm{s},2}} \tag{5.9}$$

with the varying chord Reynolds number are shown in Figures 5.7 and 5.8, respectively. The data points of all the cases (i.e. the cases where the low Reynolds numbers are achieved by both downscaling the compressor geometry and varying the compressor inlet conditions) are fitted to the power function. The R^2 values of the power function for the total pressure loss coefficient are 0.91 and 0.94 for the compressors with and without splitter blades, respectively. The R^2 values of the power function for the pressure recovery coefficient are 0.85 and 0.92 for the compressors with and without splitter blades, respectively. The error bars in Figures 5.7 and 5.8 present the discretisation error.

In addition to the total pressure loss and pressure recovery coefficients of the diffuser, the decrease in the Reynolds number affects the efficiency of the entire compressor stage. Figure 5.9 presents the relative change in the total-to-total isentropic efficiency with the correction equations of Table 2.1 and the numerical results of the compressor with splitter blades. The discretisation error in the numerical results is marked with the error bars. According to the results, the performance of the compressor decreases with respect to the decreasing Reynolds number quite precisely as in the correction equation published by Dietmann and Casey (2013). Based on the theoretical background of the correction equations presented in sub-chapter 2.1 and the trend of the numerical results in Figure 5.9,

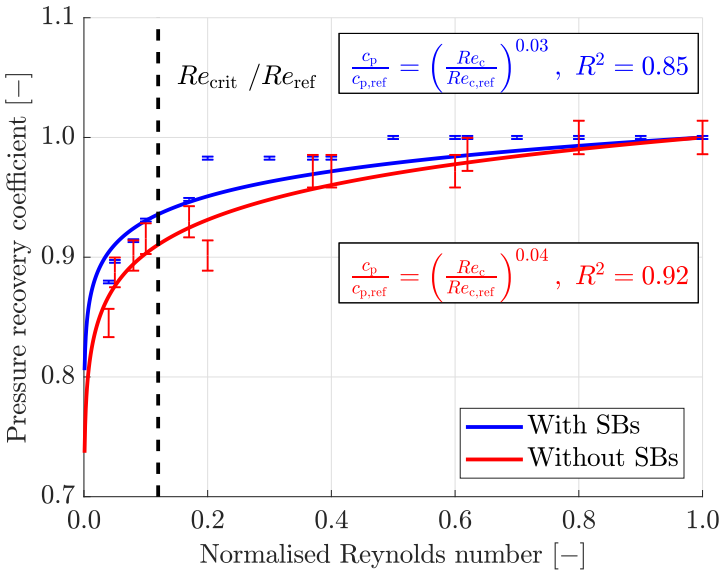

Figure 5.8: Change in a normalised pressure recovery coefficient with a varying Reynolds number. $R^2 = 0.85$ with splitter blades (SBs) and $R^2 = 0.92$ without splitter blades.

the correction equation of Dietmann and Casey (ibid.) is suggested as the most suitable correction equation for estimating the effect of the Reynolds number. The empirical correction equation also validates the trend of the numerical results, as the numerical model is validated against experimental data only at the baseline chord Reynolds number.

The change in the normalised total-to-total isentropic efficiency with the varying Reynolds number is presented in Figures 5.10 and 5.11 for the compressors with and without splitter blades, respectively. Figures 5.10 and 5.11 include two sets of numerical data: the data marked by a blue line presents the results modelled without the viscous work term in the total energy equation, and the data marked by a red line presents the results modelled with the viscous work term. The error bars present the discretisation error, and the power functions are fitted to the numerical data. The R^2 values are presented in Figures 5.10 and 5.11 for the data sets with and without the viscous work term. The numerical results are compared to the correction equation of Dietmann and Casey (2013), which is marked with a black line. The two data sets in Figures 5.10 and 5.11 are presented in order to illustrate the difference between the results published in **Publications I** and **II** and this thesis.

In **Publications I** and **II**, the compressors were erroneously modelled without the viscous work term in the total energy equation, and therefore, the results in Figures 5.9, 5.10 and 5.11 differ slightly from those presented in **Publications I** and **II**. As the boundary layer thickness increases with the decreasing Reynolds number, the efficiency was overpredicted relatively more at the low Reynolds numbers, and the numerical results deviated

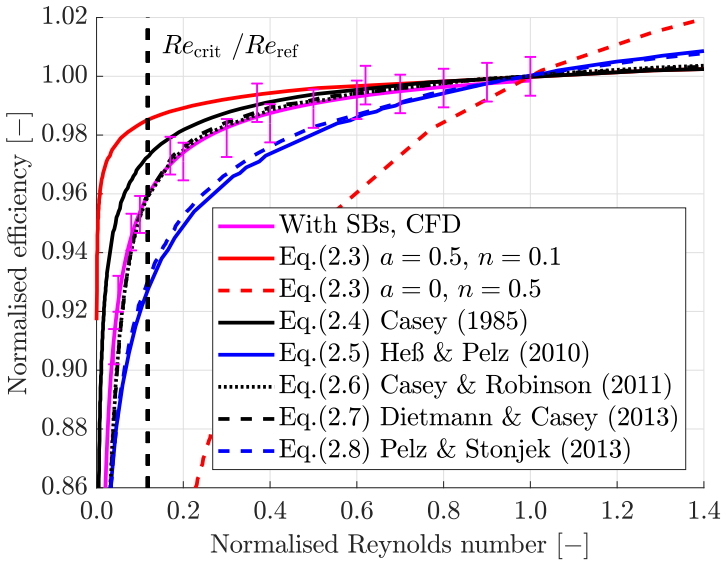

Figure 5.9: Relative change in the efficiency with a varying Reynolds number estimated with the correction equations presented in Table 2.1 and the numerical results of the compressor with splitter blades.

by $3.6-4.6\%$ from the empirical correction equations at the lowest investigated Reynolds number. In **Publication I**, the difference between the numerical results and the correction equation was explained by the neglected manufacturing tolerances, and in **Publication II** by the neglected volute and the two-equation models, which underestimated the viscous losses relatively more due to relatively increased boundary layer thickness. Manufacturing tolerances, i.e. the relatively thicker blades and larger tip clearances, would affect the efficiency of micro-scale compressors, but not large-scale compressors operating at low Reynolds numbers. Therefore, the conclusion of **Publication II** was not incorrect, as the model under-estimated the viscous losses due to the missing viscous work term in the total energy equation.

When the viscous work term was accounted for in the total energy equation, the additional efficiency decrease was on average 0.6% and maximum 2.6% at the 96% lower Reynolds number in the compressor with splitter blades (Figure 5.10). In the compressor without splitter blades, the additional efficiency decrease was on average 1.5% and maximum 5.6% at the 96% lower Reynolds number (Figure 5.11). Taking the transition into account by using the SST $k-\omega$ model in combination with the $\gamma - Re_\theta$ transition model proposed by Langtry and Menter (2005) did not change the results from the fully turbulent solution. The transition model could capture the laminar separation, but because the flow separation near the blade leading edge resulted from the centrifugal force, and not from the laminar separation, the modelling of transition in the low-Reynolds-number centrifugal compressor did not bring added value. To conclude, the results presented above demonstrate that more viscous losses occur at the low Reynolds numbers due to the

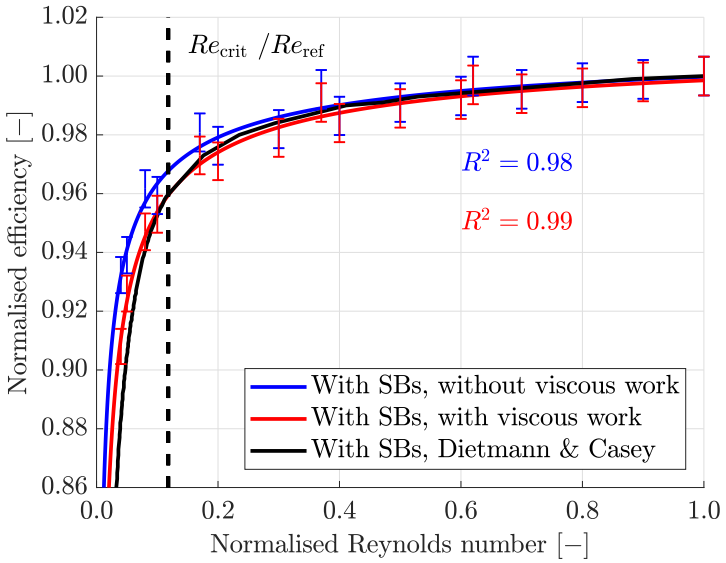

Figure 5.10: Relative change in the efficiency with a varying Reynolds number for the compressor with splitter blades. The numerical results are compared to the correction equation of Dietmann and Casey (2013).

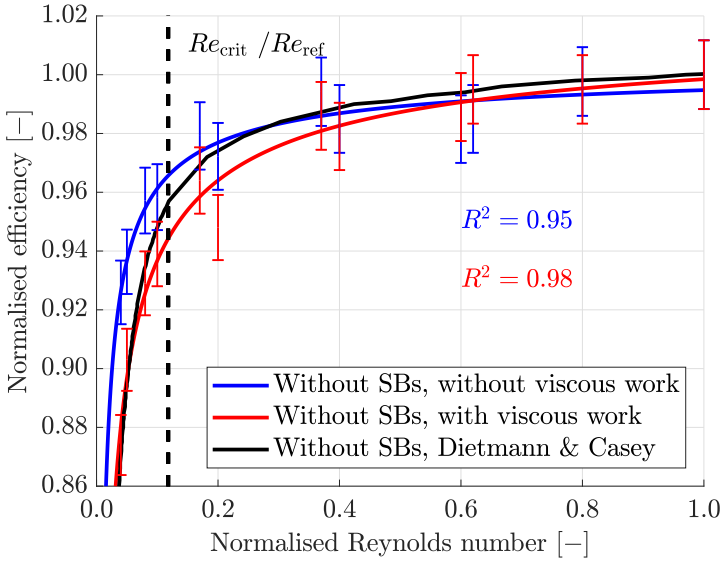

Figure 5.11: Relative change in the efficiency with a varying Reynolds number for the compressor without splitter blades. The numerical results are compared to the correction equation of Dietmann and Casey (2013).

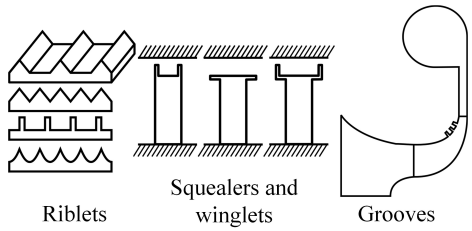

Figure 5.12: Passive flow control methods for boundary layer control (riblets) and tip leakage control (squealers, winglets, grooves).

thicker boundary layers.

5.4 Review of relevant flow control methods for low-Reynolds-number compressors

The performance of low-Reynolds-number compressors could be improved by dealing with the most significant loss generation mechanisms, i.e. the boundary layer losses, as shown in the previous sub-chapters. The decrease in the Reynolds number strengthens the tip leakage flow, and in the micro-scale compressors, the relatively larger tip clearance causes additional increase in the tip leakage losses. The performance of the low-Reynolds-number compressors could be improved with flow control methods, which were reviewed in **Publication IV**. Flow control methods are used in numerous engineering applications to improve performance and/or widen the operating range. The methods can be divided into categories based on the working purpose; whether they control separation, reduce drag, augment lift, control tip leakage, and/or improve the surge margin.

As summarised in **Publication IV**, the flow control method should increase the performance of low-Reynolds-number centrifugal compressors by reducing drag or tip leakage, whereas separation control is not a significant feature. The applicable flow control methods for controlling the boundary layers are active control methods and riblets, whereas the applicable methods for tip leakage control are squealers, winglets, and grooves. The flow control method should meet both aerodynamic and structural demands, but it cannot be structurally complex. The passive methods meet these demands and those which could improve the performance of low-Reynolds-number centrifugal compressors, are shown in Figure 5.12, namely riblets, squealers, winglets and grooves. However, the performance of the passive methods depends on the operating conditions and might be negative at higher Reynolds numbers and off-design operating conditions. Therefore, as concluded in **Publication IV**, none of the methods reviewed in **Publication IV** fulfill fully the objective of the flow control method that would reduce the boundary layer thickness and result in a reduced wake in the entire compressor operating range.

6 Conclusions and discussion

The research in this thesis concentrated on a theoretical and numerical study on loss generation in low-Reynolds-number centrifugal compressors, because especially micro-scale compressors have great potential for efficiency improvement. An improvement in the efficiency of low-Reynolds-number centrifugal compressors could increase the technological feasibility of various applications, e.g. micro-scale gas turbines.

Usually the design of a micro-scale compressor is based on a downscaled version of a larger compressor, and the performance deterioration of the downscaled compressor is estimated with empirical correction equations. Based on the theoretical background of the correction equations and the trends of the numerical results, the first main finding of this thesis and **Publication I** was that the correction equation of Dietmann and Casey (2013) is the most suitable correction equation for estimating the effect of the Reynolds number on the efficiency of the downscaled compressor. As the empirical correction equation of Dietmann and Casey (ibid.) is based on experimental data from over 30 compressors, it was used for validation in this work.

In **Publication I** it was speculated that the increased vorticity with the decreased Reynolds number and reduced compressor size due to high rotational speeds were the reasons for the performance deterioration. Therefore, the influence of the Reynolds number variation method on loss generation was studied in **Publication II**, in which the Reynolds number was varied by changing the inlet conditions instead of the compressor size. The vorticity increased in the downscaled compressor due to the smaller size, not due to the lower Reynolds number, disproving the speculations presented in **Publication I**. The second main finding (**Publication II**) was that the loss generation equals between the cases in which the low Reynolds numbers are achieved either by downscaling the compressor size or varying the compressor inlet conditions. Therefore, it seems that the losses related to a low Reynolds number should be similar regardless of the machine geometry, i.e. a low Reynolds number increases the viscous losses and tip leakage in centrifugal compressors, radial pumps and turbines.

The weakness of the correction equations is that they only account for the decrease in performance, but do not offer any consideration of whether the efficiency drop can be countered in the design process. Therefore, the third main finding of this thesis (and **Publication V**) was that the greatest increase in the Reynolds-number losses occurred in the boundary layers near the impeller hub and diffuser surfaces, and the tip leakage losses increased with the decreased Reynolds number when the relative tip clearance remained constant. In micro-scale centrifugal compressors with relatively larger tip clearances, the tip leakage losses would increase even more.

The most significant loss generation mechanism inside the compressor could not have been found without the development of a method for estimating the boundary layer thickness in the complex flow field inside the centrifugal compressor blade passage. The de-

velopment of the hybrid method was presented in Chapter 4 and **Publication III**, and it made it possible to analyse the losses inside the centrifugal compressor with a more sophisticated approach than in **Publications I** and **II**.

As mentioned in sub-chapter 5.4 and **Publication IV**, the increased boundary layer losses near the impeller hub and diffuser surfaces could be dealt with the flow control methods designed for boundary layer control, i.e. active control methods and riblets, and the tip leakage losses could be dealt with squealers, winglets and grooves. Based on aerodynamic and structural demands, the active control methods are difficult to apply to micro-scale compressors due to their complexity. On the other hand, as summarised in **Publication IV**, the drawback of passive methods is that their performance depends on the operating conditions and might be negative at higher Reynolds numbers and off-design operating conditions. An ideal flow control method would reduce the boundary layer thickness in the entire operating range of the low-Reynolds-number compressor.

Based on the conclusions presented above, the performance deterioration of micro-scale compressors due to low Reynolds numbers could be countered with flow control methods at least in one operating point, but in addition to Reynolds number losses, the manufacturing tolerances result in a relative increase in the blade thickness, tip clearance and surface roughness, which deteriorate the performance further. Therefore, the manufacturing of micro-scale centrifugal compressors does not seem profitable due to their inferior performance at present. However, new additive manufacturing and polishing technologies could be potential solutions to prevent additional losses due to relatively larger blade thicknesses, tip clearances or surface roughnesses in micro-scale machines.

However, the small size of the compressor is not necessarily problematic. Even if not studied specifically in this work, dense gases could be a potential option for the medium in micro-scale centrifugal compressors. Based on a confidential research report by the Laboratory of Fluid Dynamics at Lappeenranta University of Technology, a refrigerant like R134a resulted in Reynolds numbers higher than the critical one of $200,000$ even in micro-scale compressors (impeller outlet diameter less than 30 mm) due to the density of 10 to 20 times the air density. Schiffmann and Favrat (2009) measured total-to-total isentropic efficiencies up to 79% of a centrifugal compressor with the impeller outlet diameter of 20 mm and the medium of refrigerant R134a. The same compressor was tested in an Organic Rankine Cycle -driven heat pump with refrigerant R134a as the medium (Demierre et al., 2015), but the experimental results showed deteriorated performance due to the heat flux from the turbine. Therefore, as a recommendation for future research, small electrically-driven heat pumps could be a potential application for micro-scale centrifugal compressors without low-Reynolds-number or heat transfer losses.

As a further recommendation for future work, studies on different applications and operating conditions would make the hybrid method more general, because the hybrid model is not limited to radial turbomachines only, but should be applicable to axial machines as well.

References

ASME PTC 10 (1997). *ASME PTC 10 Performance Test Code on Compressors and Exhauster*. New York: The American Society of Mechanical Engineers. p. 188.

Backman, J. and Kaikko, J. (2011). Microturbine Systems for Small Combined Heat and Power (CHP) Applications. In: Beith, R., ed., *Small and Micro Combined Heat and Power (CHP) Systems*, chap. 7, pp. 147–178. Woodhead Publishing Series in Energy. Woodhead Publishing. ISBN 978-1-84569-795-2.

Bareiß, S., Vogt, D.M., and Chebli, E. (2015). Investigation on the Impact of Circumferential Grooves on Aerodynamic Centrifugal Compressor Performance. In: *Proceedings of ASME Turbo Expo 2015: Turbine Technical Conference and Exposition*. Paper No. GT2015-42211, p. 11. June 15–19, 2015, Montreal, Canada.

Biester, M.O., Wiegmann, F., Guendogdu, Y., and Seume, J. (2013). Time-Resolved Numerical Study of Axial Gap Effects on Labyrinth-Seal Leakage and Secondary Flow in a LP Turbine. In: *Proceedings of the ASME Turbo Expo 2013: Turbine Technical Conference and Exposition*. Paper No. GT2013-95628, p. 11. June 3–7, 2013, San Antonio, Texas, United States.

Bousquet, Y., et al. (2013). Description of the Unsteady Flow Pattern from Peak Efficiency to Near Surge in a Subsonic Centrifugal Compressor Stage. In: Backman, J., Bois, G., and Leonard, O., eds, *Proceedings of the 10th European Conference on Turbomachinery: Fluid Dynamics and Thermodynamics*, pp. 917–927. April 15–19, 2013, Lappeenranta, Finland.

Bousquet, Y., et al. (2014). Analysis of the Unsteady Flow Field in a Centrifugal Compressor from Peak Efficiency to Near Stall with Full-Annulus Simulations. *International Journal of Rotating Machinery*, 2014. doi:10.1155/2014/729629. Article ID 729629, p. 11.

Casey, M. (1985). The Effects of Reynolds Number on the Efficiency of Centrifugal Compressor Stages. *Journal of Engineering for Gas Turbines and Power*, 107, pp. 541–548. doi:10.1115/1.3239767.

Casey, M., Krähenbuhl, D., and Zwyssig, C. (2013). The Design of Ultra-High-Speed Miniature Centrifugal Compressors. In: Backman, J., Bois, G., and Leonard, O., eds, *Proceedings of the 10th European Conference on Turbomachinery: Fluid Dynamics and Thermodynamics*, pp. 506–519. April 15–19, 2013, Lappeenranta, Finland.

Casey, M. and Robinson, C. (2011). A Unified Correction Method for Reynolds Number, Size, and Roughness Effects on the Performance of Compressors. *Proceedings of the Institution of Mechanical Engineers, Part A: Journal of Power and Energy*, 225(7), pp. 864–876. doi:10.1177/0957650911410161.

Celeroton (2018). [In Celeroton www-pages]. [retrieved January 25, 2018]. From: https://www.celeroton.com/en/products/compressors.html.

Celik, I., et al. (2008). Procedure for Estimation and Reporting of Uncertainty Due to Discretization in CFD Applications. *Journal of Fluids Engineering*, 130(7). doi: 10.1115/1.2960953. Article ID 078001, p. 4.

Choi, M., et al. (2008). Effects of the Low Reynolds Number on the Loss Characteristics in an Axial Compressor. *Proceedings of the Institution of Mechanical Engineers, Part A: Journal of Power and Energy*, 222, pp. 209–218. doi:10.1243/09576509JPE520.

Coleman, H. (2009). *ASME V&V 20-2009 Standard for Verification and Validation in Computational Fluid Dynamics and Heat Transfer*. American Society of Mechanical Engineers. ISBN 978-0791832097. p. 100.

Cumpsty, N.A. and Horlock, J.H. (2006). Averaging Nonuniform Flow for a Purpose. *Journal of Turbomachinery*, 128(1), pp. 120–129. doi:10.1115/1.2098807.

Demierre, J., Rubino, A., and Schiffmann, J.A. (2015). Modeling and Experimental Investigation of an Oil-Free Micro Compressor-Turbine Unit for an ORC Driven Heat Pump. *Journal of Engineering for Gas Turbines and Power*, 137(3). doi:10.1115/1.4028391. Article ID 032602, p. 10.

Denton, J.D. (1993). Loss Mechanisms in Turbomachines. *Journal of Turbomachinery*, 115, pp. 621–656. doi:10.1115/1.2929299.

Dessornes, O., et al. (2014). Advances in the Development of a Microturbine Engine. *Journal of Engineering for Gas Turbines and Power*, 136(7). doi:10.1115/1.4026541. Article ID 071201, p. 9.

Dietmann, F. and Casey, M. (2013). The Effects of Reynolds Number and Roughness on Compressor Performance. In: Backman, J., Bois, G., and Leonard, O., eds, *Proceedings of the 10th European Conference on Turbomachinery: Fluid Dynamics and Thermodynamics*, pp. 532–542. April 15–19, 2013, Lappeenranta, Finland.

Ding, L., et al. (2013). Experimental Investigation of the Casing Treatment Effects on Steady and Transient Characteristics in an Industrial Centrifugal Compressor. *Experimental Thermal and Fluid Science*, 45, pp. 136–145. doi: 10.1016/j.expthermflusci.2012.10.016.

Durante, A., et al. (2017). Thermodynamic Simulation of a Multi-Step Externally Fired Gas Turbine Powered by Biomass. *Energy Conversion and Management*, 140, pp. 182 – 191. ISSN 0196-8904, doi:10.1016/j.enconman.2017.02.050.

Eckardt, D. (1976). Detailed Flow Investigations Within a High-Speed Centrifugal Compressor Impeller. *Journal of Fluids Engineering*, 98(3), pp. 390–399. doi: 10.1115/1.3448334.

the Parliamentary Committee on Energy and Issues, C. (2014). *Energy and Climate Roadmap 2050 – Report of the Parliamentary Committee on Energy and Climate Issues*

on 16 October 2014. Publications of the Ministry of Employment and the Economy. Energy and the climate 50/2014. ISBN 978-952-227-906-4, p. 77.

Epstein, A., Jacobson, S.A., Protz, J.M., and Frechette, L.G. (2000). Shirtbutton-Sized Gas Turbines: The Engineering Challenges of Micro High Speed Rotating Machinery. In: *Proceedings of the 8th International Symposium on Transport Phenomena and Dynamics of Rotating Machinery (ISROMAC-8)*. March 26–30, 2000, Honolulu, Hawaii, USA.

the European Commission (2012a). [In the European Commission www-pages]. [retrieved December 18, 2017]. From: https://ec.europa.eu/energy/en/topics/energy-strategy-and-energy-union/2030-energy-strategy.

the European Commission (2012b). [In the European Commission www-pages]. [retrieved December 18, 2017]. From: https://ec.europa.eu/energy/en/topics/energy-strategy-and-energy-union/2050-energy-strategy.

FISCHER Engineering Solutions AG (2017). [In FISCHER Engineering Solutions AG www-pages]. [retrieved January 25, 2018]. From: http://www.fischerspindle.com/facilities/fischer-engineering-solutions-ag/.

Gibson, L., Galloway, L., Kim, S.i., and Spence, S. (2017). Assessment of Turbulence Model Predictions for a Centrifugal Compressor Simulation. *Journal of the Global Power and Propulsion Society*, 1, pp. 142–156. doi:10.22261/2II890.

Guo, Q., et al. (2007). Numerical Simulations of Stall Inside a Centrifugal Compressor. *Proceedings of the Institution of Mechanical Engineers, Part A: Journal of Power and Energy*, 221(5), pp. 683–693. doi:10.1243/09576509JPE417.

Hagelstein, D., et al. (2000). Experimental and Numerical Investigation of the Flow in a Centrifugal Compressor Volute. *Journal of Turbomachinery*, 122(1), pp. 22–31. ISSN 0889504X, doi:10.1115/1.555423.

Harrison, S. (1990). Secondary Loss Generation in a Linear Cascade of High-Turning Turbine Blades. *Journal of Turbomachinery*, 112, pp. 618–624. doi:10.1115/1.2927702.

Hergt, A., Meyer, R., and Engel, K. (2006). Experimental Investigation of Flow Control in Compressor Cascades. In: *Proceedings of ASME Turbo Expo 2006: Power for Land, Sea and Air*. Paper No. GT2006-90415, p. 10. May 8–11, 2006, Barcelona, Spain.

Heß, M. and Pelz, P. (2010). On Reliable Performance Prediction Of Axial Turbomachines. In: *Proceedings of ASME Turbo Expo 2010: Power for Land, Sea and Air*, vol. 7, PARTS A, B, AND C, pp. 139–149. Paper No. GT2010-22290. June 14–18, 2010, Glasgow, UK.

Huttunen, R., ed., (2014). *Government Report on the National Energy and Climate Strategy for 2030 (Unofficial translation)*. Publications of the Ministry of Economic Affairs and Employment. Energy 12/2017. ISBN 978-952-327-199-9, p. 121.

the International Energy Agency (2017). [In the International Energy Agency www-pages]. [retrieved January 3, 2018]. From: http://www.iea.org/publications/freepublications/publication/Energy_Efficiency_2017.pdf.

ISO 5389 (2005). *Turbocompressors - Performance test code*. Geneve: International Organization for Standardization. p. 142.

Isomura, K., et al. (2006). Experimental Verification of the Feasibility of a 100 W Class Micro-Scale Gas Turbine at an Impeller Diameter of 10 mm. *Journal of Micromechanics and Microengineering*, 16(9), pp. S254–S261. doi:10.1088/0960-1317/16/9/S13.

Jaatinen-Värri, A., et al. (2013a). Experimental Study of Centrifugal Compressor Tip Clearance and Vaneless Diffuser Flow Fields. *Proceedings of the Institution of Mechanical Engineers, Part A: Journal of Power and Energy*, 227(8), pp. 885–895. doi: 10.1177/0957650913497358.

Jaatinen-Värri, A., et al. (2013b). The Tip Clearance Effects on the Centrifugal Compressor Vaneless Diffuser Flow Fields at Off-Design Conditions. In: Backman, J., Bois, G., and Leonard, O., eds, *Proceedings of the 10th European Conference on Turbomachinery: Fluid Dynamics and Thermodynamics*, pp. 972–982. April 15–19, 2013, Lappeenranta, Finland.

Jansen, W. (1967). A Method for Calculating the Flow in a Centrifugal Impeller When Entropy Gradients Are Present. In: *Royal Society Conference on Internal Aerodynamics (Turbomachinery)*, pp. 133–146. Paper No. 12. July 19–21, 1967. UK, Cambridge.

Japikse, D. (1996). *Centrifugal Compressor Design and Performance*. Wilder (VT): Concepts ETI. ISBN 0-933283-03-2, appr. 500 p. p. appr. 500.

Kang, S., et al. (2003). Micro-Scale Radial-Flow Compressor Impeller Made of Silicon Nitride - Manufacturing and Performance. In: *Proceedings of ASME Turbo Expo 2003: Power for Land, Sea, and Air*, vol. 3, pp. 779–788. Paper No. GT2003-38933. June 16–19, 2003, Atlanta, Georgia, USA.

Klausner, E. and Gampe, U. (2014). Evaluation and Enhancement of a One-dimensional Performance Analysis Method for Centrifugal Compressors. In: *Proceedings of ASME Turbo Expo 2014: Turbine Technical Conference and Exposition*. Paper No. GT2014-25141, p. 11. June 16–20, 2014, Düsseldorf, Germany.

Langtry, R. and Menter, F. (2005). Transition Modeling for General CFD Applications in Aeronautics. In: *43rd AIAA Aerospace Sciences Meeting and Exhibit*. Paper No. AIAA 2005-522. January, 10 – 13, 2005, Reno, Nevada.

Liu, Z. and Hill, D.L. (2000). Issues Surrounding Multiple Frames of Reference Models for Turbo Compressor Applications. In: *Proceedings of the Fifteenth International Compressor Engineering Conference*, pp. 71 – 80. Paper 1369. July 25 – 28, 2000. West Lafayette, IN, USA.

Lynch, S. and Thole, K. (2016). Comparison of the Three-Dimensional Boundary Layer on Flat Versus Contoured Turbine Endwalls. *Journal of Turbomachinery*, 138. doi: 10.1115/1.4032165. Article ID 041008, p. 10.

Marcellan, A., Visser, W., and Colonna, P. (2016). Potential of Micro Turbine Based Propulsion Systems for Civil UAVs: A Case Study. In: *Proceedings of the ASME Turbo Expo: Turbomachinery Technical Conference and Exposition*. Paper No. GT2016-57719, p. 10. June 13 – 17, 2016, Seoul, South Korea.

Martinez, S., Michaux, G., Salagnac, P., and Bouvier, J.L. (2017). Micro-Combined Heat and Power Systems (Micro-CHP) Based on Renewable Energy Sources. *Energy Conversion and Management*, 154(Supplement C), pp. 262 – 285. ISSN 0196-8904, doi: 10.1016/j.enconman.2017.10.035.

Menter, F. (2009). Review of the Shear-Stress Transport Turbulence Model Experience from an Industrial Perspective. *International Journal of Computational Fluid Dynamics*, 23(4), pp. 305–316. doi:10.1080/10618560902773387.

Moody, L.F. (1925). The Propeller Type Turbine. *Proceedings of the American Society of Civil Engineers*, 51, pp. 1009–1031.

Mühlemann, E. (1948). Zur Aufwertung des Wirkungsgrades von Ueberdruck-Wasserturbinen. *Schweizerische Bauzeitung*, 66(24), pp. 331–333. doi:10.5169/seals-56732.

Official Statistics of Finland (OSF) (2017). Energy Supply and Consumption [e-publication]. ISSN=1799-7976. 2016. Helsinki: Statistics Finland [retrieved: December 18, 2017]. From: http://www.stat.fi/til/ehk/2016/ehk_2016_2017-12-08_tie_001_en.html.

Pelz, P. and Stonjek, S. (2013). The Influence of Reynolds Number and Roughness on the Efficiency of Axial and Centrifugal Fans - a Physically Based Scaling Method. *Journal of Engineering for Gas Turbines and Power*, 135(5). doi:10.1115/1.4022991. Article ID 052601, p. 8.

Prust Jr., H.W. (1973). Boundary-Layer Losses. In: Glassman, A.J., ed., *Turbine Design and Application*, vol. 2, chap. 7, pp. 93–122. Washington, D.C.: National Aeronautics and Space Administration. NASA SP–290.

Rodgers, C. (1980). Specific Speed and Efficiency of Centrifugal Impellers. In: *Proceedings of the Twenty-fifth Annual International Gas Turbine Conference and Exhibit and Twenty-second Annual Fluids Engineering Conference*, pp. 191–200. March 9–13, 1980. New Orleans, Louisiana, USA.

Röyttä, P., Turunen-Saaresti, T., and Honkatukia, J. (2009a). Optimising the Refrigeration Cycle with a Two-Stage Centrifugal Compressor and a Flash Intercooler. *International Journal of Refrigeration*, 32(6), pp. 1366–1375. doi:10.1016/j.ijrefrig.2009.01.006.

Röyttä, P., et al. (2009b). Effects of Different Blade Angle Distributions on Centrifugal Compressor Performance. *International Journal of Rotating Machinery*, 2009. doi: 10.1155/2009/537802. Article ID 537802, p. 9.

Schiffmann, J. and Favrat, D. (2009). Experimental Investigation of a Direct Driven Radial Compressor for Domestic Heat Pumps. *International Journal of Refrigeration*, 32(8), pp. 1918–1928. ISSN 0140-7007, doi:10.1016/j.ijrefrig.2009.07.006.

Schleer, M. and Abhari, R.S. (2005). Influence of Geometric Scaling on the Stability and Range of a Turbocharger Centrifugal Compressor. In: *Proceedings of ASME Turbo Expo 2005: Power for Land, Sea, and Air*, pp. 859–869. Paper No. GT2005-68713. June 6–9, 2005, Reno, Nevada, USA.

Schlichting, H. (1979). *Boundary-Layer Theory*, 7th edn. New York: McGraw-Hill Book Company. 817 p. Translation of: Grenzschicht-Theorie. Transl. by J. Kestin. ISBN 0-07-055334-3.

Seo, J., et al. (2017). Development and Experimental Investigation of a 500-W Class Ultra-Micro Gas Turbine Power Generator. *Energy*, 124(Supplement C), pp. 9 – 18. ISSN 0360-5442, doi:10.1016/j.energy.2017.02.012.

Shahin, I., Alqaradawi, M., Gadala, M., and Badr, O. (2017). On the Aero Acoustic and Internal Flows Structure in a Centrifugal Compressor with Hub Side Cavity Operating at Off Design Condition. *Aerospace Science and Technology*, 60, pp. 68–83. doi:10.1016/j.ast.2016.10.031.

Smirnov, P., Hansen, T., and Menter, F. (2007). Numerical Simulation of Turbulent Flows in Centrifugal Compressor Stages with Different Radial Gaps. In: *Proceedings of the ASME Turbo Expo 2007: Power for Land, Sea and Air*, pp. 1029–1038. Paper No. GT2007-27376, p. 10. May14–17, 2007, Montreal, Canada.

Smith, N.R., Berdanier, R.A., Fabian, J.C., and Key, N.L. (2015). Reconciling Compressor Performance Differences for Varying Ambient Inlet Conditions. *Journal of Engineering for Gas Turbines and Power*, 137(12). doi:10.1115/1.4030518. Article ID 122603, p. 9.

Sun, Z., Tan, C., and Zhang, D. (2009). Flow Field Structures of the Impeller Backside Cavity and Its Influences on the Centrifugal Compressor. In: *Proceedings of ASME Turbo Expo 2009: Power for Land, Sea and Air*, pp. 1349–1360. Paper No. GT2009-59879. June 8–12, 2009, Orlando, Florida, USA.

Turunen-Saaresti, T. and Jaatinen, A. (2013). Influence of the Different Design Parameters to the Centrifugal Compressor Tip Clearance Loss. *Journal of Turbomachinery*, 135. doi:10.1115/1.4006388. Article ID 011017, p. 6.

Turunen-Saaresti, T., Reunanen, A., and Larjola, J. (2006). Computational and Experimental Study of Pinch on the Performance of a Vaneless Diffuser in a Centrifugal

Compressor. *Journal of Thermal Science*, 15(4), pp. 306–313. ISSN 1003-2169, doi: 10.1007/s11630-006-0306-1.

the United Nations (2015). [In the United Nations www-pages]. [retrieved December 15, 2017]. From: http://www.un.org/sustainabledevelopment.

Visser, W., et al. (2012). Performance Optimization of a 3kW Microturbine for CHP Applications. In: *Proceedings of ASME Turbo Expo 2012: Turbine Technical Conference and Exposition*, vol. 5, pp. 619–628. Paper No. GT2012-68686. June 11-15, 2012, Copenhagen, Denmark.

Vittorini, D. and Cipollone, R. (2016). Energy Saving Potential in Existing Industrial Compressors. *Energy*, 102, pp. 502 – 515. ISSN 0360-5442, doi: 10.1016/j.energy.2016.02.115.

Vogel, K., Abhari, R.S., and Zemp, A. (2015). Experimental and Numerical Investigation of the Unsteady Flow Field in a Vaned Diffuser of a High-Speed Centrifugal Compressor. *Journal of Turbomachinery*, 137(7). doi:10.1115/1.4029175. Article ID 071008, p. 9.

Weber, A., Schreiber, H.A., Fuchs, R., and Steinert, W. (2002). 3-D Transonic Flow in a Compressor Cascade With Shock-Induced Corner Stall. *Journal of Turbomachinery*, 124, pp. 358–366. doi:10.1115/1.1460913.

Weber, A., et al. (2016). Flow Analysis of a High Flowrate Centrifugal Compressor Stage and Comparison With Test Rig Data. In: *Proceedings of ASME Turbo Expo 2016: Turbomachinery Technical Conference and Exposition*. Paper No. GT2016-56551, p. 12. June 13–17, 2016, Seoul, South Korea.

Wiesner, F.J. (1979). A New Appraisal of Reynolds Number Effects on Centrifugal Compressor Performance. *Journal of Engineering for Gas Turbines and Power*, 101(3), pp. 384–392. doi:10.1115/1.3446586.

Wilcox, D. (1994). *Turbulence Modeling for CFD*. California: La Cañada. P. 460. ISBN 0-9636051-0-0.

Wright, T. (1989). Comments on Compressor Efficiency Scaling with Reynolds Number and Relative Roughness. In: *Proceedings of the Gas Turbine and Aeroengine Congress and Exposition 1989*. Paper No. GT31, p. 7. June 4–8, 1989, Toronto, Canada.

Xu, W., Wang, T., Gu, C., and Ding, L. (2011). A Study on the Influence of Hole's Diameter With Holed Casing Treatment. In: *Proceedings of ASME Turbo Expo 2011*, vol. 4, pp. 499–508. Paper No. GT2011-46167. June 6–10, 2011, Vancouver, British Columbia, Canada.

Yamada, K., et al. (2010). Comparative Study on Tip Clearance Flow Fields in Two Types of Transonic Centrifugal Compressor Impeller with Splitter Blades. In: *Proceedings of*

ASME Turbo Expo 2010: Power for Land, Sea and Air, vol. 7, PARTS A, B, AND C, pp. 2053–2063. Paper No. GT2010-23345. June 14-18, 2010, Glasgow, UK.

Yang, M., et al. (2012). Stability Improvement of High-Pressure-Ratio Turbocharger Centrifugal Compressor by Asymmetric Flow Control-Part I: Non-Axisymmetrical Flow in Centrifugal Compressor. *Journal of Turbomachinery*, 135(2). doi:10.1115/1.4006636.

Zheng, X., et al. (2013). Effects of Reynolds Number on the Performance of a High Pressure-Ratio Turbocharger Compressor. *Science China: Technological Sciences*, 56(6), pp. 1361–1369. ISSN 1674-7321, doi:10.1007/s11431-013-5213-6.

Ziegler, K. (2003). *CFD Test Case Centrifugal Compressor "Radiver" with MTU Impeller of Aachen University: Readme-file of the Test Case CD-ROM*. Version 1.0, 30.09.2003.

Ziegler, K., Gallus, H., and Niehuis, R. (2003). A Study on Impeller-Diffuser Interaction - Part I: Influence on the Performance. *Journal of Turbomachinery*, 125(1), pp. 173–182. doi:10.1115/1.1516814.

ACTA UNIVERSITATIS LAPPEENRANTAENSIS

766. LAAKKONEN, JUSSI. An approach for distinct information privacy risk assessment. 2017. Diss.

767. KASURINEN, HELI. Identifying the opportunities to develop holistically sustainable bioenergy business. 2017. Diss.

768. KESKISAARI, ANNA. The impact of recycled raw materials on the properties of wood-plastic composites. 2017. Diss.

769. JUKKA, MINNA. Perceptions of international buyer-supplier relational exchange. 2017. Diss.

770. BAYGILDINA, ELVIRA. Thermal load analysis and monitoring of doubly-fed wind power converters in low wind speed conditions. 2017. Diss.

771. STADE, SAM. Examination of the compaction of ultrafiltration membranes with ultrasonic time-domain reflectometry. 2017. Diss.

772. KOZLOVA, MARIIA. Analyzing the effects of a renewable energy support mechanism on investments under uncertainty: case of Russia. 2017. Diss.

773. KURAMA, ONESFOLE. Similarity based classification methods with different aggregation operators. 2017. Diss.

774. LYYTIKÄINEN, KATJA. Removal of xylan from birch kraft pulps and the effect of its removal on fiber properties, colloidal interactions and retention in papermaking. 2017. Diss.

775. GAFUROV, SALIMZHAN. Theoretical and experimental analysis of dynamic loading of a two-stage aircraft engine fuel pump and methods for its decreasing. 2017. Diss.

776. KULESHOV, DMITRII. Modelling the operation of short-term electricity market in Russia. 2017. Diss.

777. SAARI, JUSSI. Improving the effectiveness and profitability of thermal conversion of biomass. 2017. Diss.

778. ZHAO, FEIPING. Cross-linked chitosan and β-cyclodextrin as functional adsorbents in water treatment. 2017. Diss.

779. KORHONEN, ILKKA. Mobile sensor for measurements inside combustion chamber – preliminary study. 2017. Diss.

780. SIKIÖ, PÄIVI. Dynamical tree models for high Reynolds number turbulence applied in fluid-solid systems of 1D-space and time. 2017. Diss.

781. ROMANENKO, ALEKSEI. Study of inverter-induced bearing damage monitoring in variable-speed-driven motor systems. 2017. Diss.

782. SIPILÄ, JENNI. The many faces of ambivalence in the decision-making process. 2017. Diss.

783. HAN, MEI. Hydrodynamics and mass transfer in airlift bioreactors; experimental and numerical simulation analysis. 2017. Diss.

784. ESCALANTE, JOHN BRUZZO. Dynamic simulation of cross-country skiing. 2017. Diss.

785. NOKKA, JARKKO. Energy efficiency analyses of hybrid non-road mobile machinery by real-time virtual prototyping. 2018. Diss.

786. VUORIO, ANNA. Opportunity-specific entrepreneurial intentions in sustainable entrepreneurship. 2018. Diss.

787. PULKKINEN, AKI. Towards a better understanding of activity and selectivity trends involving K and O adsorption on selected metal surfaces. 2017. Diss.

788. ZHAO, WENLONG. Reliability based research on design, analysis and control of the remote handling maintenance system for fusion reactor. 2018. Diss.

789. IAKOVLEVA, EVGENIA. Novel sorbents from low-cost materials for water treatment. 2018. Diss.

790. KEDZIORA, DAMIAN. Service offshoring industry: systems engineering approach to its transitional challenges. 2018. Diss.

791. WU, JING. Soft computing methods for performance improvement of EAMA robot in fusion reactor application. 2018. Diss.

792. VOSTATEK, PAVEL. Blood vessel segmentation in the analysis of retinal and diaphragm images. 2018. Diss.

793. AJO, PETRI. Hydroxyl radical behavior in water treatment with gas-phase pulsed corona discharge. 2018. Diss.

794. BANAEIANJAHROMI, NEGIN. On the role of enterprise architecture in enterprise integration. 2018. Diss.

795. HASHEELA-MUFETI, VICTORIA TULIVAYE. Empirical studies on the adoption and implementation of ERP in SMEs in developing countries. 2018. Diss.

796. JANHUNEN, SARI. Determinants of the local acceptability of wind power in Finland. 2018. Diss.

797. TEPLOV, ROMAN. A holistic approach to measuring open innovation: contribution to theory development. 2018. Diss.

798. ALBATS, EKATERINA. Facilitating university-industry collaboration with a multi-level stakeholder perspective. 2018. Diss.

799. TURA, NINA. Value creation for sustainability-oriented innovations: challenges and supporting methods. 2018. Diss.

800. TALIKKA, MARJA. Recognizing required changes to higher education engineering programs' information literacy education as a consequence of research problems becoming more complex. 2018. Diss.

801. MATTSSON, ALEKSI. Design of customer-end converter systems for low voltage DC distribution from a life cycle cost perspective. 2018. Diss.

802. JÄRVI, HENNA. Customer engagement, a friend or a foe? Investigating the relationship between customer engagement and value co-destruction. 2018. Diss.

803. DABROWSKA, JUSTYNA. Organizing for open innovation: adding the human element. 2018. Diss.